Aus der

Berufsgenossenschaftlichen Unfallklinik

Klinik für Unfall- und Wiederherstellungschirurgie an der
Universität Tübingen

Effects of Berberine, a Natural Plant-Derived DPP4 Inhibitor, on In Vitro Scab Remodeling

Inaugural-Dissertation
zur Erlangung des Doktorgrades
der Medizin

der Medizinischen Fakultät
der Eberhard-Karls-Universität
zu Tübingen

vorgelegt von

Yuan, Sanhuan

2026

Dekan: Professorin Dr. S. Y. Brucker

1. Berichterstatter: Professorin Dr. S. Ehnert
2. Berichterstatter: Professorin Dr. C. Weigert

Tag der Disputation: 12.10.2026

To my mother and father

Table of contents

List of abbreviations VI

List of figures VIII

List of tables IX

1. Introduction 1

1.1. Diabetes and impaired wound healing 1

1.2. Anatomy and physiology of the skin 2

1.2.1. Epidermis 2

1.2.2. Dermis 3

1.2.3. Subcutis 3

1.3. The wound healing process 4

1.3.1. Hemostasis and fibrin clot formation 5

1.3.2. Inflammation 5

1.3.3. Proliferation: re-epithelialization and phenotypic remodeling 6

1.3.4. Remodeling and tissue maturation 7

1.4. Experimental models of wound healing 9

1.5. DPP4-mediated epithelial-mesenchymal transition in wound healing 10

1.6. Pharmacological properties of berberine and its therapeutic potential in wound healing 15

1.7. Study Objectives and Hypotheses 17

2. Materials and Methods 18

2.1. Materials 18

2.1.1. Human blood and serum samples 18

2.1.2. Cell line (HaCaT) 18

2.1.3. Chemicals and Reagents 18

2.1.4. Buffers, medium and solutions 19

2.1.5. Kits and assay systems 20

2.1.6. Consumables 20

2.1.7. Instruments and equipment 20

2.2. Methods 22

2.2.1. Preparation of *in vitro* scab models 22

2.2.2. Scab phenotype analysis (weight and size measurement) 23
2.2.3. Gene expression analysis by reverse transcription PCR (RT-PCR) 24
2.2.4. Protein level analysis by ELISA 27
2.2.5. DPP4 inhibitor screening assay 28
2.2.6. Drug treatments and interventions 29
2.2.7. Cell viability and cytotoxicity assays 29
2.2.8. Statistical analyses 30
3. Results 31
3.1. Diabetes impairs remodeling of the *in vitro* scabs 31
3.2. Dysregulated EMT in DM scabs 32
3.2.1. Enhanced expression of epithelial markers in DM scabs 32
3.2.2. Low expression of mesenchymal markers in DM scabs 33
3.2.3. Expression of EMT transcription factors is affected in DM scabs 34
3.2.4. Assessment of matrix metalloproteinases (MMPs) and inhibitor expression 35
3.3. Study cohort characterization 36
3.3.1. Increased expression of DPP4 in DM scabs 36
3.3.2. Systemic upregulation of DPP4 in Pre-DM and DM patients 37
3.3.3. Clinical characteristics of the study cohort 38
3.3.4. Hematological characteristics of the study cohort 39
3.4. Addition of exogenous DPP4 impaired scab remodeling 40
3.5. BBR inhibits DPP4 and promotes scab remodeling 41
3.5.1. Pharmacological validation of BBR as a DPP4 inhibitor 41
3.5.2. Cytotoxicity assessment of BBR with scabs 42
3.5.3. BBR restores remodeling dynamics in DM scabs 43
3.6. BBR effects on EMT in DM scabs 44
3.6.1. BBR lowers DPP4 and epithelial marker expression in DM scabs 44
3.6.2. BBR induces expression of mesenchymal markers in DM scabs 45
3.6.3. BBR normalizes key EMT transcription factors in DM scabs 46
4. Discussion 48
4.1. Impaired scab remodeling in diabetes 48
4.2. Dysregulated EMT as a key mechanism in diabetic wound healing 49
4.3. DPP4 as a critical regulator of scab remodeling 51

4.4. BBR as a natural DPP4 inhibitor 51
4.5. Context-dependent effects and dosing considerations 53
4.6. Limitations of the study 54
4.7. Outlook and future directions 55
4.8. Conclusions 57
5. Summary 59
6. Zusammenfassung 60
7. Bibliography 62
8. Appendix A 72
Molecular effects of BBR on gene expression in control scabs 72
9. Declaration 75
10. Publication 76
11. Acknowledgement 77

List of abbreviations

3D	three dimensional
ANOVA	analysis of variance
ADA	adenosine deaminase
AMPK	AMP-activated protein kinase
AUC	area under the curve
BBR	berberine
BMI	body mass index
$CaCl_2$	calcium chloride
cDNA	complementary DNA
COL1A1	collagen type I alpha 1
DAMPs	detect damage-associated molecular patterns
ddH2O	double distilled H2O
DEPC	diethyl pyrocarbonate
DETCs	dendritic epidermal T cells
DMEM	dulbecco's Modified Eagle's Medium
DMSO	dimethyl sulfoxide
DPP4	dipeptidyl peptidase-4
ECM	extracellular matrix
EDTA	ethylenediaminetetraacetic acid
EMT	epithelial-mesenchymal transition
E-cadherin	epithelial cadherins
ELISA	enzyme-linked immunosorbent assay
FBS	fetal bovine serum
FCS	fetal calf serum
FN	fibronectin
GLP-1	glucagon-like peptide-1
GIP	glucose-dependent insulinotropic polypeptide

HbA1c	hemoglobin A1c
KGF	keratinocyte growth factor
MCHC	mean corpuscular hemoglobin concentration
MCH	mean corpuscular hemoglobin
MCV	mean corpuscular volume
MAPKs	mitogen-activated protein kinases
MMPs	matrix metalloproteinases
NF-κB	nuclear factor-κB
NO	nitric oxide
Nrf2	nuclear factor erythroid 2-related factor 2
PAMPs	pathogen-associated molecular patterns
PAR2	protease-activated receptor-2
PBS	phosphate buffered saline
PCR	polymerase chain reaction
PDGF	platelet-derived growth factor
PRRs	pattern recognition receptors
rhDPP4	recombinant human DPP4
ROS	oxygen species
RT-PCR	Reverse Transcription PCR
sDPP4	soluble dipeptidyl peptidase-4
SDF-1α	stromal cell-derived factor-1α
TCR	T-cell receptor
TIMPs	tissue inhibitors of metalloproteinases
TrxR1	thioredoxin reductase 1
TNF-α	tumor necrosis factor alpha
TGF-β	transforming growth factor beta
VEGF	vascular endothelial growth factor
vWF	von Willebrand factor

List of figures

Figure 1: Schematic illustration of human skin anatomy 4

Figure 2: The four overlapping phases of wound healing 8

Figure 1: Structural and functional composition of the *in vitro* scab model……10

Figure 4: Proposed therapeutic mechanisms of DPP4 inhibitors in promoting chronic wound healing……...15

Figure 5: The experimental flowchart for the construction of *in vitro* scab model. 23

Figure 6: Delayed remodeling in DM scabs. 32

Figure 7: Compared to control scabs, DM scabs show enhanced expression of epithelial markers. 33

Figure 8: Compared to control scabs, DM scabs show lower expression of mesenchymal markers. 34

Figure 9: Dysregulated expression of EMT transcription factors in DM scabs. 35

Figure 10: Expression of *MMP1*, *MMP2*, *MMP9*, *TIMP1* and *TIMP2* in scabs. 36

Figure 11: Systemic and local upregulation of DPP4 in DM. 38

Figure 12: Clinical anthropometric characteristics of the study cohort. 39

Figure 13: Hematological characteristics of the study cohort. 40

Figure 14: Modulation of DPP4 activity alters scab remodeling kinetics in control scabs. 41

Figure 15: Dose-dependent inhibition of DPP4 activity by BBR. 42

Figure 16: Cytotoxicity assessment of BBR in *in vitro* scabs. 43

Figure 17: BBR restores remodeling dynamics in diabetic scabs. 44

Figure 18: BBR attenuates *DPP4* and epithelial marker expression in DM scabs. 45

Figure 19: BBR induces pro-mesenchymal marker expression in diabetic scabs. 46

Figure 20: BBR normalizes EMT transcription factor expression in diabetic scabs. 47

Figure A1: Effects of BBR on *DPP4* and epithelial marker expression in control scabs……73

Figure A2: Effects of BBR on mesenchymal marker expression in control scabs……73

Figure A3: Effects of BBR on EMT transcription factor expression in control scabs……74

List of tables

Table 1: List of used chemicals 18

Table 2: List of used solutions 19

Table 3: List of used kits 20

Table 4: List of used consumables 20

Table 5: List of used equipment 20

Table 6: Specifications of F: Forward and R: Reverse primers used in gene expression analysis 26

Table 7: Baseline characteristics of patients (Scab Phenotype) 32

Table 8: Baseline characteristics of patients (ELISA) 37

1. Introduction

1.1. Diabetes and impaired wound healing

Diabetes mellitus (DM) constitutes one of the most important metabolic concerns globally. According to forecasts from the International Diabetes Federation (IDF), the number of individuals with diabetes worldwide will exceed 700 million by 2045 (International Diabetes Federation 2025, Saeedi *et al*. 2020). This disease has a tremendous burden of complications. Among them, diabetic chronic wounds (such as diabetic foot ulcers) are distinguished by their prolonged length, poor healing rates, and high likelihood of recurrence. These wounds represent a prominent cause of non-traumatic amputation and premature death (Boulton *et al*. 2005). They substantially degrade patient quality of life and create substantial economic expenses (Armstrong *et al*. 2017).

The primary difficulty in diabetic wound healing involves pathological changes of the local repair environment. Chronic hyperglycemia increases oxidative stress, stimulates continuous release of pro-inflammatory cytokines, and alters cellular energy metabolism. These alterations disrupt the physiological balance essential for wound repair (Giacco *et al*. 2010, Singh *et al*. 2005). As a result, the four stages of healing, comprised of hemostasis, inflammation, proliferation, and remodeling, undergo sequential malfunction. For example, poor macrophage polarization might trap wounds in a persistent inflammatory state. The wounds fail to shift correctly to the proliferative phase (Mirza *et al*. 2014). At the same time, insulin resistance greatly lowers glucose use by repair-related cells. This decreases the proliferation and migratory capacity of fibroblasts and endothelial cells. As a result, the creation and maturation of granulation tissue are prevented (Liu *et al*. 2009).

Furthermore, poor angiogenesis exacerbates tissue hypoxia and nutritional deficit. Metabolic toxicity from the high-glucose environment directly impairs

arterial endothelial function. It also alters the bioavailability of essential molecules such as nitric oxide (NO), hence limiting the repair of the microcirculation (Kolluru *et al*. 2012). This microvascular dysfunction overlaps with diabetic peripheral neuropathy. The combination may generate a vicious cycle of damage, ischemia, and infection (Vinik *et al*. 2001). Current treatment methods including debridement and dressings demonstrate little success in treating underlying metabolic and cellular dysfunctions (Hinchliffe *et al*. 2008). Notably, re-epithelialization is the ultimate phase in wound closure. This mechanism is greatly affected in the diabetic setting. As the main mechanism for epidermal barrier regeneration, keratinocytes must change their original phenotype in response to diverse signaling molecules. They must acquire migratory capacity to cover the wound (Shteingauz *et al*. 2018). However, how metabolic diseases interfere with this process through specific molecular switches remains a significant research concern. Therefore, studying the key molecular pathways is clinically critical for creating tailored therapies to restore tissue regeneration dynamics.

1.2. Anatomy and physiology of the skin

The skin is the biggest organ, acting as the dynamic interface between internal physiological balance and the external world. It orchestrates thermoregulation, barrier defense, and metabolic regulation by meticulous multilayer organization. Histologically, the skin comprises three structurally continuous layers: the epidermis, dermis, and subcutaneous tissue (Kanitakis *et al*. 2002).

1.2.1. Epidermis

The epidermis is a stratified squamous epithelium measuring 75 to 150 μm in thickness in most regions of the body. Attaining a thickness of up to 600 μm in acral regions devoid of hair follicles (Sandby-Møller *et al*. 2003). Keratinocytes constitute roughly 95% of epidermal cells. They experience vertical migration and terminal differentiation from the proliferative basal layer to the surface, resulting in the formation of five distinct horizontal strata: basal (stratum

basale), spinous (stratum spinosum), granular (stratum granulosum), clear (stratum lucidum), and cornified (stratum corneum) layers (Blanpain *et al*. 2009). The complete rejuvenation cycle requires around 25 to 45 days (Weinstein *et al*. 1984). This layer also encompasses specialized non-epithelial cells: melanocytes at the dermal-epidermal junction produce melanin for photoprotection (Yamaguchi *et al*. 2014); Langerhans cells in the spinous layer serve as antigen-presenting cells (Romani *et al*. 2010); and Merkel cells establish synaptic connections for sensory perception (Maksimovic *et al*. 2014). Structural cohesion relies on desmosomes and tight junctions that govern paracellular permeability (Figure 1) (Segre *et al*. 2006).

1.2.2. Dermis

The dermis lies beneath the surface, varying in thickness from under 1 mm in the eyelids to over 4 mm in the back (Wheater *et al*. 1987). The structure consists of the superficial papillary layer, abundant in type III collagen and capillary loops for metabolic exchange, and the deep reticular layer, which contains type I collagen bundles (comprising 80–90% of fiber content) interwoven with elastic fibers (Uitto *et al*. 1989, Braverman *et al*. 1997, Uitto *et al*. 1998). Fibroblasts produce the extracellular matrix, comprising hyaluronic acid, whereas the vascular network oversees thermoregulation (Papakonstantinou *et al*. 2012, Braverman *et al*. 2000). Additionally, the dermis contains macrophages, mast cells, and memory T cells. These form the fundamental immunological defense mechanism of the epidermal barrier (Nestle *et al*. 2009).

1.2.3. Subcutis

The subcutaneous tissue secures the skin to the fascia through adipose lobules divided by fibrous septa (Kruglikov *et al*. 2016). Adipocytes serve as endocrine cells that release adipokines, such as leptin and adiponectin (Rosen *et al*. 2006), while the micro-vesicular collagen network offers mechanical support (Mizukoshi *et al*. 2024, Sun *et al*. 2023). Subcutaneous fat distribution

exhibits notable sexual dimorphism, indicative of evolutionary variations in thermoregulation and energy reserves (Wells *et al*. 2007).

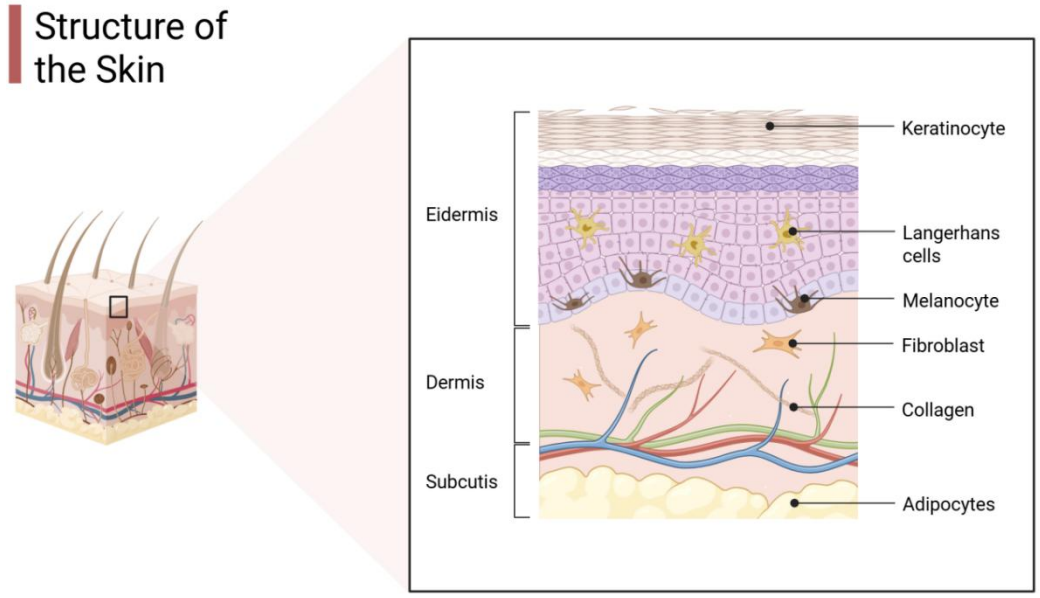


Figure 2: Schematic illustration of human skin anatomy. Cross-sectional illustration showing the three layers of human skin: the epidermis (stratified squamous epithelium containing keratinocytes, Langerhans cells, and melanocytes), the dermis (fibroblasts and collagen fibers), and the subcutis (adipocytes). The schematic illustration was generated with the assistance of BioRender and graphically adapted from a previous study (Harry *et al*. 2025).

1.3. The wound healing process

Wound healing entails a physiologically coordinated cascade involving various cell types and signaling molecules operating in exact spatial and temporal synchrony. This dynamic process is conventionally categorized into four functionally separate but temporally overlapping phases: hemostasis, inflammation, proliferation, and remodeling (Nowak *et al*. 2021). The accurate transition and physiological advancement between these phases constitute the foundation of effective mending. A failure to adequately transition from the inflammatory phase to proliferation may result in chronic wound development in situations such as diabetes (Eming *et al*. 2014). Consequently, a systematic clarification of the physiological mechanisms regulating each stage is essential for comprehending how metabolic abnormalities impede wound healing processes (Figure 2).

1.3.1. Hemostasis and fibrin clot formation

Following tissue injury, the healing process commences with hemostasis. This technique inhibits excessive hemorrhage while creating a transient physical framework for eventual cellular infiltration. Vascular injury reveals subendothelial collagen, triggering both intrinsic and extrinsic coagulation pathways. Platelets agglomerate mediated by von Willebrand factor (vWF), accompanied by localized vasoconstriction (Wolberg *et al*. 2023). The initial vasoconstrictive response generally endures for 5 to 10 minutes. The resultant localized hypoxia and pH variations paradoxically trigger first signals for tissue regeneration (Schäfer *et al*. 2008).

In this phase, a clot abundant in fibrin occupies the wound defect. This transient matrix mostly comprises polymerized fibrinogen, fibronectin, and vitronectin. In addition to acting as a hemostatic barrier, it also serves as a three-dimensional biochemical substrate that facilitates cell migration at the wound site (Heher *et al*. 2018). Concurrently, activated platelets in the clot experience degranulation, releasing various bioactive mediators, such as platelet-derived growth factor (PDGF) and transforming growth factor-β (TGF-β). These substances attract inflammatory cells via chemotaxis, therefore facilitating the physiological shift from hemostasis to inflammation (Schultz *et al*. 2009).

1.3.2. Inflammation

The inflammatory phase significantly coincides with hemostasis. It signifies the synchronized reaction of the immune system to tissue injury and possible microbial invasion. Resident skin cells, comprising keratinocytes, macrophages, dendritic cells, and mast cells, surveil injured cells via pattern recognition receptors (PRRs, including TLRs). They identify damage-associated molecular patterns (DAMPs) emitted by injured cells and pathogen-associated molecular patterns (PAMPs) from microbes (Chen *et al*. 2010). These recognition signals initiate intracellular transduction pathways,

encompassing nuclear factor-κB (NF-κB) and mitogen-activated protein kinases (MAPKs). This stimulates the expression of pro-inflammatory cytokines (including TNF-α and IL-1β) and chemokines (such as CXCL8/IL-8, CCL2/MCP-1, and CCL5/RANTES) (Hayden *et al*. 2008).

Neutrophils represent the initial influx of invading immune cells. They execute essential activities by producing proteolytic enzymes and reactive oxygen species (ROS) to eliminate infections and necrotic debris (Nathan *et al*. 2006). Under physiological conditions, neutrophils often survive for 2 to 5 days. They enhance signals by releasing inflammatory substances. Monocytes subsequently extravasate from circulation and develop into tissue macrophages. Macrophages serve a critical regulatory function during the inflammatory phase. They facilitate the change of the wound environment from a pro-inflammatory state to a reparative phenotype by eliminating leftover debris and secreting growth factors (Novak *et al*. 2013). Dendritic epidermal T cells (DETCs) also contribute to this process. They facilitate future epithelium restoration by synthesizing keratinocyte growth factor (KGF) and other mediators (Knoedler *et al*. 2023).

1.3.3. Proliferation: re-epithelialization and phenotypic remodeling

As inflammatory signals diminish, the proliferative phase becomes predominant. The fundamental characteristics encompass re-epithelialization, angiogenesis, and the formation of granulation tissue. The fibronectin-rich matrix serves as a scaffold for cellular migration (Shahin *et al*. 2025).

During re-epithelialization, keratinocytes at the wound margin exhibit significant epithelial plasticity. The absence of contact inhibition and exposure to signals from wounds trigger a partial epithelial-to-mesenchymal transition (EMT), during which cells diminish intercellular adhesion structures like E-cadherin and desmosomes, restructure their actin cytoskeleton, and gain migratory abilities. This process entails the activation of early signaling driven by Keratin 18, cytoskeletal remodeling induced by reduced amounts of Keratin

19, and the release of the extracellular segment of Syndecan 1 from the cell membrane (Sun *et al*. 2023). Migrating leading-edge cells produce matrix metalloproteinases, such as MMP-9, to cleave Syndecan 1 and disintegrate compromised basement membrane components, thereby circumventing physical barriers (Michopoulou *et al*. 2020). Concurrently, Keratin 19-positive epidermal stem cells in skin appendages provide cellular reserves by proliferation. They progressively reconstruct the basement membrane during migration to reestablish barrier function (Rittié *et al*. 2013). Exact regulation of this phenotypic alteration is essential for re-epithelialization. Any element that impedes this plasticity may result in unsuccessful repair. The hypoxic milieu of the wound bed stimulates HIF-1α signaling concurrently with epithelial healing. This enhances the expression of vascular endothelial growth factor (VEGF), promoting angiogenesis (Hong *et al*. 2014). Endothelial cells penetrate the aged basement membrane by the activity of proteases. They generate new capillary buds by proliferation and migration, thereby restoring local blood perfusion (Lustig *et al*. 2009). In the deep dermis, fibroblasts are attracted to the provisional matrix by chemokines like PDGF and TGF-β, where they produce substantial quantities of extracellular matrix abundant in type III collagen and hyaluronic acid. Following mechanical stimulation, some fibroblasts develop into myofibroblasts. They diminish the wound area through their contractile action. The resultant granulation tissue offers structural framework and biochemical signaling support for ultimate restoration (Werner *et al*. 2003).

1.3.4. Remodeling and tissue maturation

Upon the maturation of granulation tissue, the conclusive remodeling phase commences. This pathophysiological process may persist for months to years. In this phase, the cellular composition of the wound approaches stability and resolution. Upon the release of mechanical strain, myofibroblasts experience programmed cell death. Superfluous microvascular networks progressively

diminish by vessel pruning. These coordinated actions finally reestablish metabolic equilibrium (Merkt *et al*. 2021).

The essence of remodeling encompasses enhancement of quality and development of the extracellular matrix. Type III collagen, initially deposited, is progressively substituted by type I collagen, which possesses greater tensile strength, under the meticulous management of matrix metalloproteinases (MMPs) and their inhibitors (TIMPs). This enzymatic turnover facilitates the organized alignment and cross-linking of collagen strands. The tensile strength of repaired tissue can ultimately restore to 80% of the original skin strength (Verhaegen *et al*. 2009). Nevertheless, highly specialized skin appendages, like hair follicles and sweat glands, typically do not achieve complete regeneration in adult wounds. This results in repaired tissue exhibiting functional and cosmetic differences compared to undamaged skin. The efficacy of repair relies on a dynamic equilibrium between matrix deposition and degradation. When this equilibrium is disrupted, it inevitably results in hypertrophic scarring or enduring chronic wounds (Ogawa *et al*. 2011).

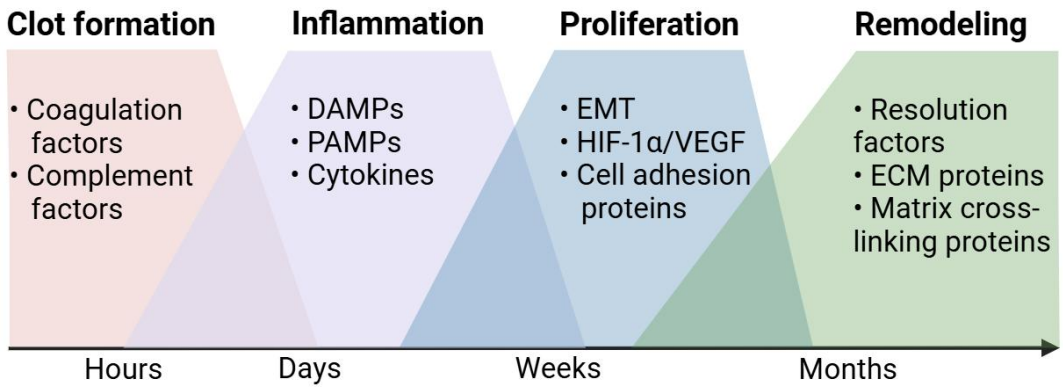


Figure 3: The four overlapping phases of wound healing. The wound healing process comprises four functionally distinct but temporally overlapping phases: clot formation (hours), involving coagulation and complement cascade activation; inflammation (days), characterized by recognition of DAMPs/PAMPs and cytokine release; proliferation (weeks), featuring EMT, HIF-1α/VEGF-driven angiogenesis, and cell adhesion dynamics; and remodeling (months), encompassing resolution factors, ECM protein turnover, and matrix cross-linking. The schematic illustration was generated with the assistance of BioRender and graphically adapted from a previous study (Peña *et al.* 2025).

1.4. Experimental models of wound healing

Skin restoration is intricate, encompassing phases of inflammation, proliferation, and tissue remodeling that are temporally coordinated. Consequently, resilient experimental systems are essential for mechanistic investigation and therapeutic assessment (Sullivan *et al*. 2001). Preclinical wound healing models encompass both *in vitro* cell culture methods and *in vivo* animal models. Each category possesses distinct advantages and inherent restrictions.

In vivo models are crucial for investigating the whole biological mechanisms of tissue restoration. Rodents, especially mice and rats, are extensively utilized due to their comprehensive array of cell types and clearly delineated genetic origins. Nevertheless, they predominantly depend on wound contraction as the principal mechanism of closure. This markedly contrasts with human healing, which primarily relies on re-epithelialization and the creation of granulation tissue (Ansell *et al*. 2012). Large-animal models, such as rabbits and pigs, more accurately reflect human skin structure and healing dynamics. The rabbit ear chamber model efficiently inhibits wound contraction via cartilage fixation. This enables quantitative evaluation of novel tissue deposition (Sharun *et al*. 2024). Nonetheless, technical intricacy and resource demands limit its extensive implementation (Sotomayor *et al*. 2017). Porcine models exhibit significant parallels with human skin architecture and immunological responses. Nonetheless, ethical concerns and maintenance expenses restrict their regular application (Summerfield *et al*. 2015).

Simultaneously, *in vitro* techniques have seen continual evolution. Conventional two-dimensional scratch experiments and sophisticated three-dimensional (3D) organotypic cultures enable the examination of cell migration and matrix interactions (Liang *et al*. 2007). Nonetheless, these systems intrinsically lack hematological and immunological elements essential for early wound physiology. They are unable to reproduce the formation of the fibrin clot and scab, together with their biological functions (Xue *et al*. 2015).

To rectify shortcomings in current models, we have developed an innovative *in vitro* scab model. This model combines human keratinocytes (HaCaT cell line) with fresh human whole blood. It employs the fibrin network generated by normal blood coagulation as a three-dimensional biological scaffold. This effectively summarizes the physiological milieu of early wound closure (Liu *et al*. 2022). Introducing entire blood components allows encapsulated immune cells within the fibrin network to release diverse cytokines. This replicates genuine dynamic interactions between skin cells and blood constituents (Figure 3).

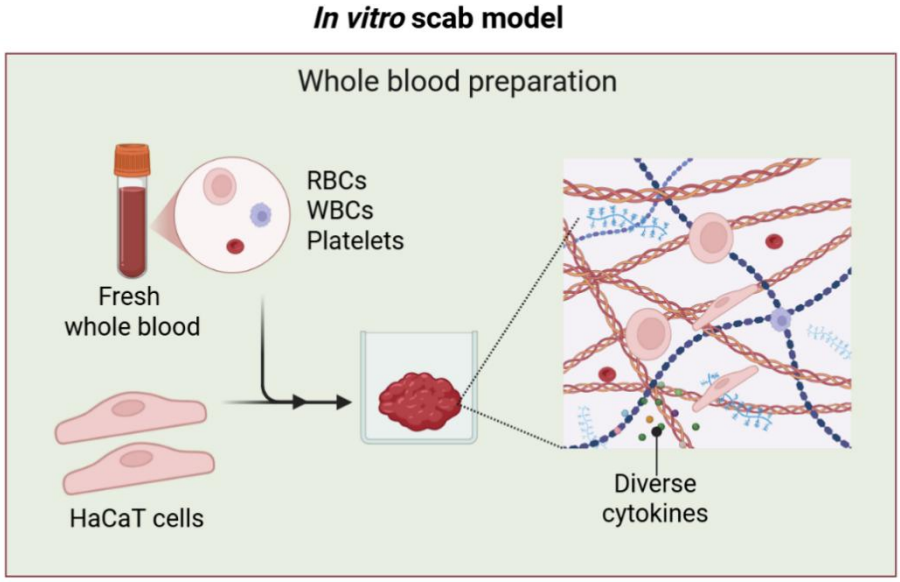


Figure 4: Structural and functional composition of the *in vitro* scab model. This model integrates human keratinocytes (HaCaT cells) with fresh whole blood, utilizing the natural fibrin network as a three-dimensional biological scaffold to simulate the physiological milieu of early wound closure (Liu *et al*. 2022). The inclusion of complete blood components (RBCs, WBCs, and platelets) enables encapsulated immune cells within the fibrin matrix to release diverse cytokines, facilitating dynamic interactions between skin cells and blood constituents. The schematic illustration was generated with the assistance of BioRender and graphically adapted from a previous study (Liu *et al*. 2022).

1.5. DPP4-mediated epithelial-mesenchymal transition in wound healing

Dipeptidyl peptidase-4 (DPP4) is a highly conserved, multifunctional transmembrane enzyme system. It exists in two separate molecular structures *in vivo*. These represent the membrane-associated and soluble variants. This imparts highly intricate biological characteristics to the molecule. DPP4 was

first discovered in liver tissue in 1966. It was later identified as the T-cell surface antigen CD26. It is a type II transmembrane glycoprotein consisting of 766 amino acids. It comprises a brief cytoplasmic tail, a singular hydrophobic transmembrane domain, and an extensively glycosylated extracellular catalytic region (Marguet *et al*. 2000). The extracellular domain is further categorized into specific regions. These facilitate accurate substrate identification, interactions with cysteine-rich proteins, and cell adhesion mediated by glycosylation (Cheng *et al*. 2003).

In addition to the conventional membrane-bound form, proteolytic cleavage by MMPs in the flexible stalk region produces a soluble variant (sDPP4). This form is present in plasma and different bodily fluids (Lambeir *et al*. 2001). This soluble isoform maintains full dipeptidase activity despite the absence of transmembrane anchoring. It has evolved into an autonomous circulating signaling molecule with unique pathophysiological implications. sDPP4 levels markedly elevate in the presence of metabolic abnormalities and chronic inflammatory conditions. This establishes a structural foundation for its fundamental regulating function in the milieu of diabetic chronic wounds (Gaggini *et al*. 2025).

The functional breadth of DPP4 transcends its recognized involvement in controlling glucose homeostasis. As a conventional serine exopeptidase, it particularly identifies and hydrolyzes N-terminal dipeptides from substrates containing proline or alanine in the penultimate position. This enzymatic mechanism swiftly deactivates incretin hormones, such as glucagon-like peptide-1 (GLP-1) and glucose-dependent insulinotropic polypeptide (GIP). Consequently, it directly influences metabolic equilibrium (Drucker et al. 2006). Nonetheless, the protein serves as a significant non-catalytic immunomodulatory scaffold. DPP4 specifically interacts with adenosine deaminase (ADA), caveolin-1, and elements of the T-cell receptor (TCR) complex via its extracellular domain. It functions as a costimulatory molecule that markedly amplifies lymphocyte activation and proliferation dynamics

(Chitadze *et al*. 2021).

Moreover, sDPP4 operates as a signaling ligand. It can attach to particular receptor systems, including protease-activated receptor-2 (PAR2) and the insulin-like growth factor II/mannose-6-phosphate receptor. This initiates downstream pathways that lead to the nuclear translocation of NF-κB and the transcription of pro-inflammatory genes. This process frequently transpires autonomously of its enzymatic function (Hui *et al*. 2023). This dual functional property may elucidate the interaction between immune cells in the blood component and epithelial cells via DPP4 in the scab model.

EMT is a reversible cellular reprogramming process marked by epithelial-mesenchymal plasticity. In the process of wound healing, keratinocytes undergo partial EMT states that facilitate migration while maintaining the intercellular adhesion necessary for collective re-epithelialization. Throughout this process, epithelial cells progressively forfeit their distinctive cobblestone shape, apical-basal polarity, and tight intercellular connections. They obtain mesenchymal biochemical traits. These encompass augmented migratory potential, invasiveness, and the capacity to modify the extracellular matrix (Kalluri *et al*. 2009). In contemporary developmental biology, this change is not a mere binary switch. Rather, it constitutes a dynamic phenotypic continuum. Partial EMT states denote extremely adaptable hybrid cellular structures. These cells retain the epithelial adhesion mechanisms essential for collective migration while developing mesenchymal motility (Nieto *et al*. 2016).

The molecular regulation of EMT depends on intricate networks of transcription factors. The families include Snail (Snail1/Snail2), ZEB (ZEB1/ZEB2), and Twist. These proteins function as sequence-specific DNA-binding repressors. They specifically target the promoters of epithelial cadherins (E-cadherin) and tight junction proteins to facilitate genetic remodeling (Stemmler *et al*. 2019). The TGF-β signaling pathway serves as the primary external regulator of EMT. It stimulates receptor serine/threonine

kinases and phosphorylates Smad proteins. This mechanism ultimately activates mesenchymal gene programs (Moustakas *et al*. 2012).

The convergence of DPP4 biology and EMT control has emerged as a pivotal mechanistic axis in skin repair physiology. In the pathogenic milieu of diabetic chronic wounds, the sustained overexpression of DPP4 correlates with compromised keratinocyte migration. Studies indicate that pharmacological reduction of DPP4 activity markedly enhances the acquisition of mesenchymal traits essential for re-epithelialization by keratinocytes (Long *et al*. 2018). The molecular foundation of this phenotypic regulation entails the localized buildup of uncleaved chemokine substrates, notably stromal cell-derived factor-1α (SDF-1α). SDF-1α activates downstream signaling pathways by interacting to its receptor CXCR4. This results in a dynamic restructuring of the cytoskeleton (Gallagher *et al*. 2007). Moreover, DPP4 inhibition seems to efficiently enhance the expression of crucial EMT transcription factors, such as Snail1 and vimentin. This allows keratinocytes to perform a regulated partial epithelial-mesenchymal transition program. This is crucial for the coordinated migration of keratinocytes across the intricate wound bed. It guarantees that cells have the requisite lateral driving force while establishing a coherent regenerating epithelial layer (Li *et al*. 2020).

DPP4 not only has direct regulatory effects on epithelial populations but also refines the quality of wound repair through its interactions with dermal fibroblasts and components generated from blood. Fibroblasts demonstrate significantly elevated DPP4 expression relative to epidermal cells. Their activation status directly affects the rate of matrix deposition and the extent of scar development ultimately (Lendahl *et al*. 2020). Inhibition of DPP4 activity in fibroblast populations markedly reduces TGF-β1-mediated endogenous signaling pathways. This mitigates the overproduction of profibrotic factors. DPP4 inhibitors simultaneously enhance the structured organization of collagen and fibronectin while elevating SDF-1α production. This paracrine pathway establishes a reciprocal signaling feedback loop within the wound

microenvironment. Multiple active factors secreted by fibroblasts and immune cells within the scab tissue, in response to DPP4 inhibition, collaborate with adjacent keratinocytes. This enhances their pro-migratory epithelial-mesenchymal transition phenotype (Sinagra *et al*. 2015). This discovery offers a significant theoretical foundation for the *in vitro* scab model utilized in this research. The model replicates interactions between blood and skin cells to more accurately examine DPP4 control of cytokines throughout scab development.

Experimental evidence and clinical translation studies collectively validate the significant therapeutic potential of targeting the DPP4-EMT regulatory axis in chronic wound treatment. Multiple preclinical investigations indicate that the use of DPP4 inhibitors in diabetic animal models markedly facilitates granulation tissue development, improves microvascular density, and expedites epithelial covering. The histological enhancements are strongly associated with increased expression of EMT markers at the molecular level and diminished pro-inflammatory cytokine levels (Schürmann *et al*. 2012). Randomized controlled trials involving human patients in clinical research have shown promising outcomes. Histological examination of diabetic foot ulcer patients treated with saxagliptin demonstrated a considerable increase in vimentin expression in keratinocytes at the lesion margin. The rate of wound healing was improved (Gao *et al*. 2025). This further illustrates that DPP4 inhibition can elicit advantageous phenotypic alteration in humans. Consequently, it mitigates repair delays induced by metabolic problems.

In conclusion, DPP4 is not only a basic metabolic regulating enzyme. This is a crucial molecular switch regulating epithelial plasticity and tissue remodeling. Its regulating function in wound healing has distinct dual therapeutic advantages. It provides keratinocytes with the migratory capacity essential for fast wound closure by initiating a regulated partial EMT. Conversely, it efficiently inhibits the buildup of fibrotic matrix that leads to pathological scarring by obstructing fibroblast activation (Zhang *et al*. 2022). The

combination action of facilitating migration and diminishing fibrosis renders DPP4 inhibitors an attractive treatment choice for addressing chronic, difficult-to-heal wounds and enhancing healing quality. In addition to focused synthetic medications, multi-target substances derived from natural sources provide a significant alternative for wound treatment (Figure 4). Berberine (BBR), an element of a traditional medicinal plant, demonstrates notable promise in modulating epithelial plasticity and inflammatory responses (Li *et al*. 2024).

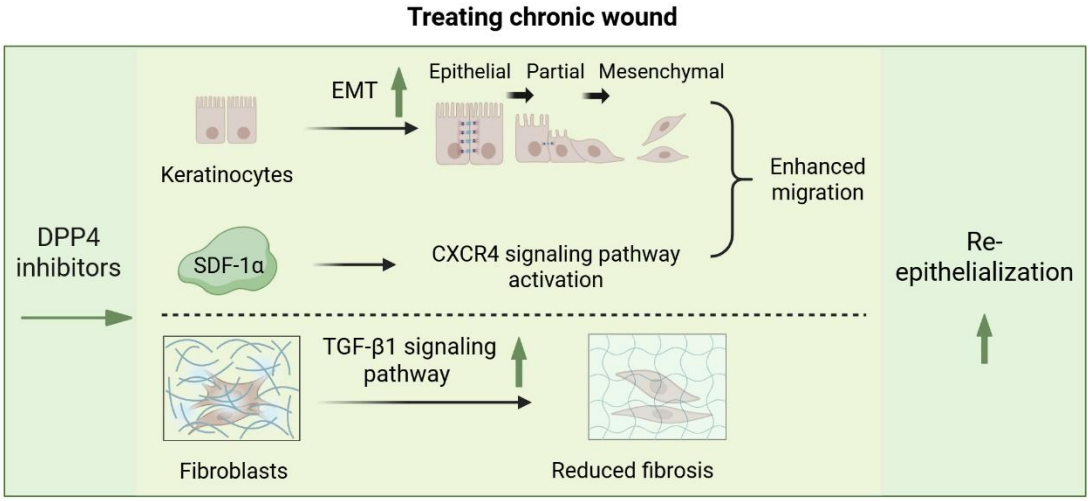


Figure 4: Proposed therapeutic mechanisms of DPP4 inhibitors in promoting chronic wound healing. DPP4 inhibitors facilitate re-epithelialization by enhancing keratinocyte migration through the induction of EMT and activation of the SDF-1α/CXCR4 signaling pathway, while concurrently reducing fibrosis in fibroblasts via modulation of the TGF-β1 signaling pathway. The schematic illustration was generated with the assistance of BioRender and graphically adapted from a previous study (Gallagher *et al*. 2007, Sinagra *et al*. 2015, Zhang *et al*. 2022).

1.6. Pharmacological properties of berberine and its therapeutic potential in wound healing

Pharmacological inhibition of DPP4 provides a focused method for altering epithelial plasticity and inflammation, whereas natural substances give additional therapeutic options with multi-target regulatory abilities. BBR, an isoquinoline alkaloid derived from the rhizomes of medicinal plants including Coptis chinensis, Berberis aristata, and Phellodendrum amurense, has emerged as a viable contender for wound therapy (Yin *et al*. 2025). Historically

employed in Chinese and Ayurvedic medicine for gastrointestinal ailments, BBR demonstrates a wide array of pharmacological properties, encompassing metabolic regulation, anti-inflammatory actions, and modulation of oxidative stress (Askari *et al*. 2023, Bellavite *et al*. 2023).

The therapeutic mechanisms of BBR entail the activation of essential cellular pathways associated with wound healing. BBR diminishes inflammatory cytokine production and bolsters antioxidant defenses in macrophages and epithelial cells by stimulating the AMP-activated protein kinase (AMPK) and nuclear factor erythroid 2-related factor 2 (Nrf2) signaling pathways (Dong *et al*. 2023). BBR significantly affects epithelial-mesenchymal transition by obstructing TGF-β1-induced phosphorylation of Smad2/3 and the ensuing nuclear translocation of Smad4. This activity aids in averting aberrant epithelial-mesenchymal transition associated with fibrosis while perhaps facilitating the temporary epithelial-mesenchymal transition required for keratinocyte migration (Huang *et al*. 2024, Huang *et al*. 2020). This pathway resembles but differs from DPP4-mediated EMT regulation, suggesting possible synergy. The therapeutic use of BBR in wound healing requires attention to its pharmacokinetic constraints. Systemic injection yields low bioavailability (absolute bioavailability <1%) due to significant first-pass metabolism and intestinal absorption impediments, further exacerbated by diabetic vascular dysfunction that limits medication delivery to ulcer locations (Pan *et al*. 2002, Feng *et al*. 2019). Topical treatment bypasses these obstacles, facilitating direct distribution to the wound site, where BBR can activate thioredoxin reductase 1 (TrxR1) to restore redox equilibrium and improve the impaired regeneration milieu typical of diabetes wounds (Liu *et al*. 2010). Consequently, BBR is a significant phytochemical supplement that facilitates wound repair via many molecular targets.

1.7. Study Objectives and Hypotheses

Overall Aim: The primary objective of this study is to investigate the molecular mechanisms underlying impaired scab remodeling in diabetic conditions and to evaluate Berberine (BBR) as a potential therapeutic intervention targeting the DPP4-EMT axis.

To achieve this aim, we propose the following hypotheses:

Hypothesis 1: Diabetic conditions delay / impair *in vitro* scab remodeling. To test this hypothesis, the change in scab size and weight over time will be compared between diabetic and non-diabetic control scabs.

Hypothesis 2: Impaired scab remodeling in diabetes is associated with dysregulated EMT. To test this hypothesis expression of EMT transcription factors, epithelial and mesenchymal markers will be assessed. According to our hypothesis diabetic scabs will show a prolonged expression of epithelial markers and a delayed expression of mesenchymal markers.

Hypothesis 3: Elevated *DPP4* expression and activity constitute a critical molecular mechanism underlying impaired EMT and delayed scab remodeling in diabetic wounds, such that (a) exogenous DPP4 impairs remodeling, and (b) DPP4 inhibition (sitagliptin) restores normal remodeling dynamics. To test this hypothesis respective stimulation and inhibition experiments will be performed.

Hypothesis 4: BBR, as a natural DPP4 inhibitor, dose-dependently inhibits DPP4 activity without cytotoxicity, restores EMT marker balance, and accelerates scab remodeling in diabetic conditions. To test this hypothesis the above described experiments will be repeated with non-toxic concentrations of BBR.

2. Materials and Methods

2.1. Materials

2.1.1. Human blood and serum samples

All blood samples were obtained from healthy volunteers and patients at the BG Clinic Tübingen. The collection of blood samples was approved by the Ethics Committee of the University Hospital Tübingen (approval no. 844/2020B02), and written informed consent was obtained from all participants prior to sample collection.

2.1.2. Cell line (HaCaT)

HaCaT cells are spontaneously immortalized human epidermal cells derived from keratinocytes, retaining the differentiation capacity of keratinocytes. HaCaT cells were obtained through a material transfer from the German Cancer Research Center (DKFZ).

2.1.3. Chemicals and Reagents

Table 1: List of used chemicals

Materials	Cat. No.	Company
Ammonium Thiocyanate	221988-100g	Sigma
Berberine chloride hydrate (≥90%)	14050	Merck
Boric acid 99.8% p.a.	6943.1	Carl Roth
Bromophenol	A512.1	Carl Roth
Calcein-AM	ABD-22002	Thermo Fisher
Calcium chloride ($CaCl_2$)	CN93.2	Carl Roth
Chloroform	Y015.1	Carl Roth
Diethylpyrocarbonate (DEPC)	K028.3	Carl Roth
Dulbecco's Phosphate Buffered Saline (DPBS)	D8537	Merck
DMEM high glucose (4.5 g/L) with L-Glutamine	D5796	Merck
Dimethyl sulfoxide (DMSO)	4720.2	Carl Roth
ddH_2O	3175.1	Carl Roth
Ethidium Bromide	2218.1	Carl Roth
FCS (Fetal Calf Serum)	10270	Thermo Fisher
Glycerol	G6376-100G	Sigma
Guanidine Thiocyanate	0017.1	Carl Roth
Hoechst 33342	H1399	Thermo Fisher

Isopropanol	33539	Honeywell
Penicillin/Streptomycin	P0781	Merck
Resazurin sodium salt	199303-1G	Merck
Roti Aqua Phenol	A980.3	Carl Roth
Sodium Acetate	X891.2	Carl Roth
Trypsin/EDTA	T3924	Merck
Trypan Blue	CN76.1	Carl Roth
Trizma base (TRIS)	T1503	Sigma

2.1.4. Buffers, medium and solutions

Table 2: List of used solutions

Items	Compounds
Berberine stock solution	37.2 mg Berberine chloride hydrate (≥90%) 1 mL DPBS
Berberine working solutions	5 µL Berberine stock solution 5 mL culture medium (scab model)
$CaCl_2$ stock solution	333.42 mg $CaCl_2$ 10 mL ddH_2O
$CaCl_2$ working solution	1 mL $CaCl_2$ stock solution 2 mL culture medium (scab model)
Calcein-AM stock solution	502 µl DMSO 1 mg Calcein AM
Coagulation medium	1 mL $CaCl_2$ stock solution 29 mL culture medium
Culture medium for HaCaT cells (5% FCS)	500 mL DMEM 25 mL Fetal Calf Serum (FCS / heat inactivated)
Culture medium for scab model (5% FCS)	500 mL DMEM 5 mL Penicillin/Streptomycin 25 mL Fetal Calf Serum (FCS / heat inactivated)
DEPC H_2O	1 mL DEPC 1 L ddH_2O
Hoechst stock solution	10 mg Hoechst 33342 5 mL DMSO
PCR loading buffer (5X)	25 mg bromphenol blue 5 mL 10X TBE 5 mL Glycerol
Resazurin stock solution (11X)	12.5 mg resazurin sodium salt 50 mL DPBS
Resazurin working solution (1X)	100 µL resazurin stock solution (11X) 1 mL medium
Sodium acetate solution	12.3 g Sodium Acetate 50 mL ddH_2O
Self-made TriFast (100 mL)	9.45 g guanidine thiocyanate

	3.04 g ammonium thiocyanate 3.3 mL sodium acetate solution 5 mL Glycerol
TBE (10X)	108 g TRIS 55 g Boric acid 99,8% p.a. 40 mL EDTA (0,5 M) pH 8
Trypan blue solution	62.5 mg Trypan blue 50 mL Dulbecco's PBS

2.1.5. Kits and assay systems

Table 3: List of used kits

Kits	Cat. No.	Company
ELISA MAX™ Deluxe Set Human CD26 (DPP4)	449304	BioLegend, San Diego, USA
DPP4 Inhibitor Screening Assay Kit	700210	Cayman, Ann Arbor, USA
Thermo Scientific™ First Strand cDNA Synthesis Kit	K1612	Thermo Fisher Scientific, Waltham, MA, USA

2.1.6. Consumables

Table 4: List of used consumables

Material	Cat. No.	Company
S-Monovette® K3 EDTA, 9 mL	02.1066.001	Sarstedt
Safety-Multifly®-Kanüle, 21G x 3/4"	85.1638.235	Sarstedt
Cell culture plates, flat bottom, 96 wells	655180	Greiner
Cell culture plates, V bottom, 96 wells	3548	Greiner
Reaction Tubes, V bottom, 15 mL	188271	Greiner
Reaction Tubes, V bottom, 50 mL	227261	Greiner
Reaction Tubes, White, 0.5 mL	72.699	SARSTEDT AG
Reaction Tubes, White, 1.5 mL	4182.1	Carl Roth
Reaction Tubes, White, 2.0 mL	2549	Carl Roth
Pipette Tips, 0.1-10 µL		Sorenson BioScience
Pipette Tips, 2-200 µL		Sarstedt
Pipette Tips, 100-1000 µL		Ratiolab

2.1.7. Instruments and equipment

Table 5: List of used equipment

Material	Cat. No.	Company
Agitator, magnetic stirrer, RH B2	06.050357	IKA-Werke GmbH
Agitator, magnetic stirrer, MR Hei-Mix L	040700340	Heidolph
Centrifuge, Stat-Spin	620E-5000-0693	Dako

Centrifuge, Megafuge (40R)	4130-7652	Thermo Fisher
Centrifuge, SIDD (58)	DD-58-1001	Scientific Industries
Electrophoresis power supplies, Power Pac (200)	285B-R05-538	Bio-Rad
Fridge +4 °C, Comfort	3523-21L	Liebherr
Fridge +4 °C, HKMT 040-01	CC00412514	Cool Compact Kühlgeräte
Freezer -20 °C, IQ500	GS51NYW41 (01)	BSH
Freezer -20 °C, Med Line	LGex3410-21K 001	Liebherr
Freezer -80 °C, 905	827860-2521	Thermo Fisher Scientific
Ice maker, AF 80	DD 8837 11 X	Scotsmen
Incubator, Heratherm OMS-60	4129-6334	Thermo Fisher
Incubator, 90-40-00-78	11-22-649	Binder GmbH
Laboratory pump (Bench), Cyclo-2	11-090-65	Carl Roth
Microcentrifuge, BN-0806-0235	C-1301B	Labnet International GmbH
Microcentrifuge, Fresco (17)	4125-0019	HERAEUS
Microscope, EVOS (fl)	91-AF-43-01	Peqlab Biotechnologie
Microscope, CELENA-X	CLX-01-00045	Logos Biosystems
Mixer, LD (76)	76-000	Labinco B.V.
Multichannel Pipette, 5 µL, 50 µL	151-620-022	Corning Co., Ltd.
Multichannel Pipette, 20 µL, 200 µL	551-630-277	Corning Co., Ltd.
Multichannel Pipette, 0.5 µL,10 µL	CH98998(4510)	Thermo Electron
Multichannel Pipette, 50 µL, 300 µL	151640033	Corning Co., Ltd.
pH meter, Five Easy (FE-20)	1232-3152-96	Mettler Toledo
Pipette controller, Pipetboy-acu	629-619	Integra
Pipette controller, Rota-Filler-3000	HAS-05119	Heathrow Scientific
Refrigerator, HKMT-04001	CC-0041-2516	Cool Compact Kühlgeräte GmbH
Refrigerator, HKMN-062-01	CC-0041-2513	Cool Compact Kühlgeräte GmbH
Safety Work Bench, Maxisave-S202018	41293949	Thermo Fisher
Scale, ABJ-120-4M	WB-114-0084	Kern &Sohn
Shaker (laboratory), ES (20)	010111-1107-0119	PeqlabBiotechnolog
Shaker (laboratory), DRS-12	11DE-090	LTF Labortechnik
Shaker (laboratory), LSE (Vortex and Mixer)	110-1260	Corning Co., Ltd
Shaker (laboratory), DRS (12)	11DE243	LTF Labortechnik
Shaker (laboratory), ES (20)	01-0111-1107-0119	PeqlabBiotechnolog
Single-channel Pipette, 2 µL, 20 µL	158230441	Corning Co., Ltd

Single-channel Pipette, 100 µL, 1000 µL	058-261-237	Corning Co., Ltd
Single-channel Pipette, 0.1 µL, 2.5 µL	P35-434B	Eppendorf
Spectrophotometer, Fluostar Omega	415-1264	BMG Labtech
Water bath, AL 25	LCB 0727-11-0094	LAUDA DR. R. WOBSER GMBH

2.2. Methods

2.2.1. Preparation of *in vitro* scab models

2.2.1.1. Culture of HaCaT cells

HaCaT cells were cultivated in T75 flasks utilizing Dulbecco's Modified Eagle's Medium (DMEM) enriched with 5% fetal bovine serum (FBS). The culture media was exchanged every 3 to 4 days, and the cells were sustained at 37 °C in a humidified environment with 5% CO_2. Cells were subcultured upon achieving approximately 80% confluence, and only those up to passage 11 were used for all tests (Boukamp *et al*. 1988).

2.2.1.2. Scab in vitro model

The *in vitro* scab was generated by combining HaCaT cells with venous blood (Figure 5). Fresh coagulation medium was prepared by adding 1 mL of 0.3 M $CaCl_2$ stock solution to 29 mL of culture medium, resulting in a final $CaCl_2$ concentration of 10 mM. HaCaT cells were detached from culture flasks using trypsin/EDTA, collected by centrifugation at 600 × g for 10 min at room temperature, and resuspended in the freshly prepared coagulation medium. A total of 60 µL of the cell suspension, adjusted to a final concentration of 5×10^5 HaCaT cells/mL, was seeded into non-adherent 96-well plates, followed by the addition of 60 µL of whole blood (collected in EDTA tubes) per well. To ensure efficient coagulation, blood samples were stored at room temperature for no longer than 4 h prior to use. The 96-well plates were then incubated at 37 °C in a humidified atmosphere containing 5% CO_2 for 1 h to allow scab formation. After incubation, the formed scabs were carefully transferred using a 1 mL pipette to fresh non-adherent 96-well plates, residual liquid was gently

removed, and 100 µL of culture medium was added to each well. A 50 µL culture medium change was carried out every two days (Pfeiffenberger *et al*. 2019).

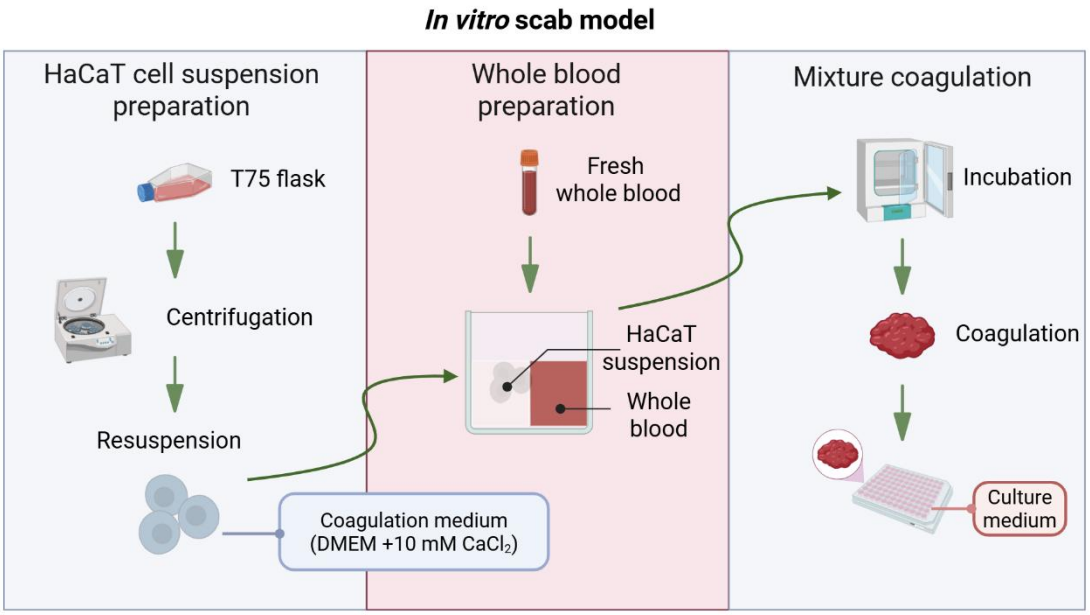


Figure 5: The experimental flowchart for the construction of *in vitro* scab model. HaCaT cells harvested from T75 flasks are concentrated via centrifugation and resuspended in coagulation medium; the cell suspension is then mixed with fresh whole blood and incubated to induce coagulation, after which the resulting scab-like structure is transferred into culture medium for further experimental analysis. The schematic illustration was generated with the assistance of BioRender and graphically adapted from a previous study (Pfeiffenberger *et al.* 2019).

2.2.2. Scab phenotype analysis (weight and size measurement)

Prior to the measurement of the weight and dimensions of the *in vitro* scabs, the culture medium was aspirated and discarded, and the scabs were transferred to a new 96-well plate. Subsequently, 50 µL of DPBS was added to each well to prevent desiccation-induced artifacts during measurement. The weight of the scabs was measured using a precision analytical balance, with a minimum of three scabs per group subjected to measurement. For dimensional analysis, the scabs were visualized and photographed under a microscope at 12.5 × magnification. The acquired images were analyzed using ImageJ software (version 1.53, USA), and the average scab diameter was calculated for quantitative assessment (Rinderknecht *et al*. 2023).

2.2.3. Gene expression analysis by reverse transcription PCR (RT-PCR)

2.2.3.1. Total RNA isolation

A minimum of twelve scabs were collected per group. The scabs were transferred to a new 96-well plate and washed with DPBS. Subsequently, the scabs were transferred to perforated columns, inserted into Eppendorf tubes, and centrifuged to homogenize the scabs. Each Eppendorf tube was supplemented with 500 µL of Trifast reagent and subsequently stored at -80 °C.

For RNA extraction, the scabs were thawed on ice and vortexed. An additional 500 µL of Trifast was added, followed by vortexing for 10 seconds. The mixture was then centrifuged at 14,000 × g for 10 minutes at 4 °C. The supernatant was carefully transferred to a new Eppendorf tube, and 200 µL of chloroform was added. The mixture was vortexed for 10 seconds and incubated at room temperature for 8 minutes.

Following incubation, the samples were centrifuged at 14,000 × g for 10 minutes at 4 °C. The upper aqueous phase was transferred to a new Eppendorf tube containing 500 µL of isopropanol. To enhance RNA precipitation, the samples were stored overnight at -20 °C.

The samples were subsequently incubated on ice for 10 minutes and centrifuged at 14,000 × g for 10 minutes at 4 °C. The RNA pellet was deposited at the bottom of the tube, and the supernatant was carefully aspirated and discarded. The RNA pellet was washed with 1 mL of 70% ethanol and centrifuged at 14,000 × g for 10 minutes at 4 °C. The supernatant was discarded, and the pellet was washed once more with 1 mL of fresh 70% ethanol under identical centrifugation conditions.

After the final wash, the supernatant was completely removed, and residual liquid at the tube opening was carefully aspirated using a micropipette. The tube caps were left open, and the samples were placed on ice for 15 minutes

to allow complete evaporation of residual ethanol. Finally, the RNA pellet was fully resuspended in 20 µL of DEPC-treated water (Liu *et al*. 2022).

2.2.3.2. RNA quantification and integrity check

RNA concentration was determined photometrically using the Omega plate reader. Based on the RNA concentrations, a reaction mixture containing 500 ng of RNA in a total volume of 5 µL was prepared. Each reaction mixture contained 1 µL of 5X loading dye (composed of 25 mg bromophenol blue, 5 mL of 10X TBE buffer, and 5 mL of 20% glycerol).

For agarose gel preparation, 1.5 g of agarose powder was dissolved in 100 mL of 1X TBE buffer by heating. Next, 7 µL of ethidium bromide was added to the molten gel. The mixture was poured into a gel casting tray and allowed to fully solidify. The prepared samples were then carefully loaded into the wells. Gel electrophoresis was conducted at a constant voltage of 70 V for 50 minutes. Samples displaying distinct and intact 18S and 28S ribosomal RNA bands were considered to be of adequate quality and were subsequently subjected to further downstream analyses (Rinderknecht *et al*. 2022).

2.2.3.3. cDNA synthesis by reverse transcription

Complementary DNA (cDNA) was synthesized using the First Strand cDNA Synthesis Kit (Thermo Fisher Scientific, USA). For each reaction, 4.5 µL of RNA template was initially combined with 1 µL of primer mixture containing oligo(dT) and random hexamer primers (0.5 µL each). Following a 5-minute incubation at 65 °C and subsequent cooling to 4 °C, 4.5 µL of reverse transcription Mastermix containing reaction buffer, Ribolock RNase inhibitor, dNTP mix, and M-MuLV reverse transcriptase was added, followed by incubation at 25 °C for 5 min, 37 °C for 60 min, and enzyme inactivation at 70 °C for 5 min, according to the manufacturer's instructions (Thermo Fisher Scientific, USA).

The resulting cDNA was diluted to a working concentration of 10 ng/µL and

stored at -20 °C for subsequent analyses. The remaining RNA samples were simultaneously preserved at -80 °C. Successful cDNA synthesis was verified by PCR amplification of the housekeeping genes RPL13α and 18S ribosomal RNA.

2.2.3.4. PCR amplification

Semi-quantitative RT-PCR was performed using 20 or 40 ng of cDNA template per reaction. The 15 µL reaction mixture consisted of 7.5 µL Red HS Taq Master Mix (Biozym, Germany), 0.75 µL each of forward and reverse gene-specific primers, and nuclease-free water. Amplification was conducted in an Applied Biosystems Veriti Thermal Cycler (Thermo Fisher Scientific, USA) under cycling conditions optimized for the respective target genes. Primer sequences and specific PCR conditions are detailed in Table 6.

Table 6: Specifications of F: Forward and R: Reverse primers used in gene expression analysis

Primer	Sequence	Size (bp)	cDNA (ng)	T_A (°C)	Cycles
DPP4	Forward: GAATGCCAGGAGGAAGGAATCT	161	20	58	35
	Reverse: CAGACCAGGACCGGAACAT				
RPL13α	Forward: AAGTACCAGGCAGTGACAG	100	20	56	30
	Reverse: CCTGTTTCCGTAGCCTCATG				
Vimentin	Forward: GTACCGGAGACAGGTGCAGT	261	20	59	35
	Reverse: TCCAGCAGCTTCCTGTAGGT				
E-cadherin	Forward: GTCAGTTCAGACTCCAGCCC	254	20	60	35
	Reverse: AAATTCACTCTGCCCAGGACG				
N-cadherin	Forward: TGGAGAACCCCATTGACATT	278	20	56	35
	Reverse: GGATTGCCTTCCATGTCTGT				
Snail1	Forward: ACCACTATGCCGCGCTCTT	115	20	62	35
	Reverse: GGTCGTAGGGCTGCTGGAA				
Snail2	Forward: ACAGCGAACTGGACACACAT	168	20	54	35
	Reverse: GAGAGAGGCCATTGGGTAGC				
Keratin 18	Forward: CCAGTCTGTGGAGAACGACA	306	20	54	35
	Reverse: TCCTCAATCTGCTGAGACCA				
Keratin 19	Forward: ACAGCCACTACTACACGACC	140	20	58	35
	Reverse: CTGTTCCGTCTCAAACTTGGTT				
Syndecan 1	Forward: GCTGAAAGGCCGGGAACC	153	40	60	35
	Reverse: CGCTCTCTACTGCCGGATTC				

ZEB1	Forward: TTACACCTTTGCATACAGAACCC Reverse: TTTACGATTACACCCAGACTGC	100	20	60	35
ZEB2	Forward: GCGATGGTCATGCAGTCAG Reverse: CAGGTGGCAGGTCATTTTCTT	138	20	62	35
MMP1	Forward: CCCAGCGACTCTAGAAACACA Reverse: TCTTGGCAAATCTGGCGTGT	322	40	60	35
MMP2	Forward: AACATACAAAGGGATTGCCAGGA Reverse: TTCAGCACAAACAGGTTGCAG	117	40	60	40
MMP9	Forward: TCTATGGTCCTCGCCCTGAA Reverse: CATCGTCCACCGGACTCAAA	219	40	64	40
TIMP1	Forward: AGTTTTGTGGCTCCCTGGAA Reverse: AAGCCCTTTTCAGAGCCTTG	179	40	60	35
TIMP2	Forward: ATGCAGATGTAGTGATCAGGGC Reverse: GTGATGTGCATCTTGCCGTC	256	40	60	35
Fibronectin	Forward: CCCCATTCCAGGACACTTCTG Reverse: GCCCACGGTAACAACCTCTT	203	20	60	35
Collagen 1A1	Forward: CAGCCGCTTCACCTACAGC Reverse: TTTTGTATTCAATCACTGTCTTGCC	83	40	60	35

2.2.3.5. Agarose gel electrophoresis and analysis of PCR products

PCR products were separated by electrophoresis on 1.5% agarose gels containing ethidium bromide. *RPL13α* was served as the housekeeping gene for normalization. Band intensities were quantified using ImageJ software. To reduce variability in loading, each sample was analyzed in duplicate.

2.2.4. Protein level analysis by ELISA

Serum DPP4 concentrations were determined by sandwich enzyme-linked immunosorbent assay (ELISA) using a commercially available human CD26 (DPP4) ELISA kit (BioLegend, USA) according to the manufacturer's protocol with minor modifications. A total of 126 serum samples were analyzed (N = 42 per group: control, pre-diabetes, and type 2 diabetes mellitus).

The lyophilized human DPP4 standard was reconstituted in 1 × Assay Diluent B to generate a 100 ng/mL stock solution, followed by preparation of a 2,000 pg/mL top standard. A five-point two-fold serial dilution series was subsequently prepared to establish the standard curve, with 1× Assay Diluent B serving as the zero standard.

Briefly, micro-well plates were coated with 100 µL of diluted capture antibody per well and incubated overnight at 4 °C. Following four washes with wash buffer, non-specific binding sites were blocked by adding 200 µL of 1 × Assay Diluent B per well and incubating at room temperature for 1 hour with shaking (500 rpm). After 4 additional washes, 100 µL of diluted standards and samples were added per well in duplicate and incubated at room temperature for 2 hours with shaking. The plates were then washed 4 times, and 100 µL of diluted detection antibody was added to each well, followed by incubation at room temperature for 1 hour with shaking. Subsequently, 100 µL of the diluted Avidin-HRP conjugate was added to each well, and the plates were incubated at room temperature with shaking for 30 minutes. After 5 washes, 100 µL of Substrate Solution D was added to each well, and the reaction was allowed to proceed in the dark for 10 minutes. The enzymatic reaction was terminated by adding 100 µL of 2N H_2SO_4 to each well.

Optical density was measured spectrophotometrically at 450 nm and 570 nm using a microplate reader (FIUO star Omega, BMG LABTECH GmbH, Germany), with the 570 nm absorbance subtracted from the 450 nm absorbance to correct for background. Protein concentrations were calculated by interpolating sample absorbance values against the standard curve using a four-parameter logistic regression model (Sahin *et al*. 2025).

2.2.5. DPP4 inhibitor screening assay

DPP4 inhibitory activity was assessed using the DPP4 Inhibitor Screening Assay Kit (Cayman Chemical, USA), a fluorescence-based enzyme inhibition assay employing Gly-Pro-AMC as the fluorogenic substrate. The assay was performed in a final volume of 100 µL per well in black 96-well plates.

The following experimental groups were established, each in triplicate: (1) background control wells containing 40 µL of diluted assay buffer and 10 µL of solvent; (2) 100% initial activity wells containing 30 µL of diluted assay buffer, 10 µL of diluted recombinant human DPP4 (DPP IV), and 10 µL of solvent; (3)

positive control wells containing 30 µL of diluted assay buffer, 10 µL of DPP4, and 10 µL of sitagliptin; and (4) test inhibitor wells containing 30 µL of diluted assay buffer, 10 µL of DPP4, and 10 µL of BBR at final concentrations of 6.25, 12.5, 25, 50, and 100 µM. Test compounds were dissolved in either assay buffer or DMSO to a final volume of 10 µL; ethanol and methanol were strictly avoided as they significantly reduce enzyme activity.

The enzymatic reactions were initiated by the addition of 50 µL of diluted substrate solution to all wells. The plate was immediately covered and incubated at 37 °C for 30 minutes. Following incubation, fluorescence intensity was measured using a microplate reader at an excitation wavelength of 350–360 nm and an emission wavelength of 450–465 nm. The mean fluorescence values were calculated for each experimental group. Background fluorescence was subtracted from both the 100% initial activity and inhibitor wells. The concentration required for 50% inhibition (IC50) was determined by nonlinear regression analysis of the dose-response curve using GraphPad Prism 9.

2.2.6. Drug treatments and interventions

For cell viability assessment, *in vitro* scabs were treated with BBR at concentrations of 6.25, 12.5, 25, 50, and 100 µM.

For mechanistic intervention experiments, scabs were exposed to recombinant human DPP4 (rhDPP4, 500 ng/mL) or to the DPP4 inhibitor sitagliptin (400 ng/mL). All treatments were administered via half-medium replacement every two days.

2.2.7. Cell viability and cytotoxicity assays

2.2.7.1. Cell viability assay

Cellular metabolic activity was quantified using the resazurin reduction assay. Briefly, scabs were transferred to fresh 96-well plates and gently rinsed with PBS until the supernatant was cleared of residual red coloration. The samples

were subsequently incubated with 100 µL of resazurin working solution (prepared by 1:11 dilution of 11 × stock solution in culture medium) at 37 °C in the dark. Following 1- and 2-hour incubation periods, 50 µL aliquots of the supernatant were transferred to a new plate, and fluorescence intensity was measured using a microplate reader (FLUOstar Omega, BMG Labtech, Germany) at excitation and emission wavelengths of 544 nm and 590 nm, respectively. Background fluorescence values were subtracted from all experimental readings (Liu *et al*. 2022).

2.2.7.2. Live/Dead cell staining

Scabs were washed three times with PBS, then transferred to fresh 96-well plates and incubated with 100 µL of culture medium containing 0.02 mM Calcein-AM at 37 °C in the dark for 10 minutes to visualize metabolically active cells. The stained samples were then examined under a fluorescence microscope using the GFP filter set (for Calcein-AM) at 200- or 400- fold magnification (Rinderknecht *et al*. 2022).

2.2.8. Statistical analyses

Statistical analyses were performed using GraphPad Prism 8 (GraphPad Software, San Diego, CA, USA). Data are presented as box-and-whisker plots showing the median, interquartile range, and all individual data points, with a significance level of $p < 0.05$. Given the small sample sizes and to maintain a robust analysis without assuming a normal distribution, non-parametric tests were employed throughout the study: the Mann-Whitney U test for two-group comparisons, and the Kruskal-Wallis test, followed by Dunn's multiple comparisons test, for multi-group analyses. Experimental groups (pre-diabetes [Pre-DM], type 2 diabetes mellitus [T2DM], or BBR-treated) were compared with their respective controls to adjust for multiple comparisons. For longitudinal wound-remodeling data, AUC was calculated from day 2 to day 14 for each sample and compared using the aforementioned non-parametric methods.

3. Results

3.1. Diabetes impairs remodeling of the *in vitro* scabs

To examine wound healing in non-diabetic control (Ctrl) and diabetic (DM) patients, we developed scab models with patient-derived whole blood. The baseline characteristics of the blood donors are given in Table 7.

Table 7: Baseline characteristics of patients (Scab Phenotype)

Variable	Control	Diabetes	p-value
Sex			1
Female	2 (33.3%)	1 (16.7%)	
Male	4 (66.7%)	5 (83.3%)	
Age (in years)	66.33 ± 12.61	64.67 ± 13.46	0.829
BMI	28.05 ± 6.27	28.30 ± 5.44	0.943
HbA1c (%)	5.25 [4.92, 5.70]	5.80 [5.60, 6.55]	0.191
C-Reactive Protein	1.99 ± 1.73	2.71 ± 2.50	0.578
Leukocytes	7200.00 ± 1451.74	7801.67 ± 1558.70	0.505
Erythrocytes	4.70 ± 0.98	4.27 ± 0.72	0.415
Hematocrit	42.68 ± 8.69	39.53 ± 8.87	0.548
Hemoglobin	14.13 ± 2.62	12.53 ± 2.80	0.331
Thrombocytes	246.67 ± 105.93	315.00 ± 98.22	0.274
INR	1.01 ± 0.06	1.01 ± 0.02	0.900
APTT	23.67 ± 3.01	24.33 ± 2.07	0.665

Data are presented as mean ± standard deviation (SD) for normally distributed variables, median [interquartile range, IQR] for non-normally distributed variables, and frequency (%) for categorical variables. Group differences between two groups were assessed using Student's t-test (parametric) or Mann-Whitney U test (non-parametric) for continuous data. Categorical variables were compared using Fisher's exact test. A p-value < 0.05 was considered statistically significant.

Morphological examination demonstrated that, at all assessed time intervals (Day 2, Day 7, and Day 14), scabs from DM patients were consistently larger than those from the control group (Figure 6A). We quantified the overall remodeling delay by calculating the area under the curve (AUC) of scab size from Day 2 to Day 14. This analysis validated the morphological observations, demonstrating a significantly elevated AUC in the DM group relative to the Ctrl group ($p < 0.0001$) (Figure 6B).

A comparable trend was noted in the fluctuations of scab weight. Throughout

the 14-day culture period, the residual weight of DM-derived scabs was markedly greater than that of Ctrl scabs (Figure 6C). The AUC analysis of weight remodeling further substantiated this conclusion, revealing that the DM group demonstrated a statistically significant increase compared to the Ctrl group ($p = 0.0032$) (Figure 6D). These quantitative results collectively indicate a significant delay and impairment in the remodeling capacity of scabs from diabetic patients.

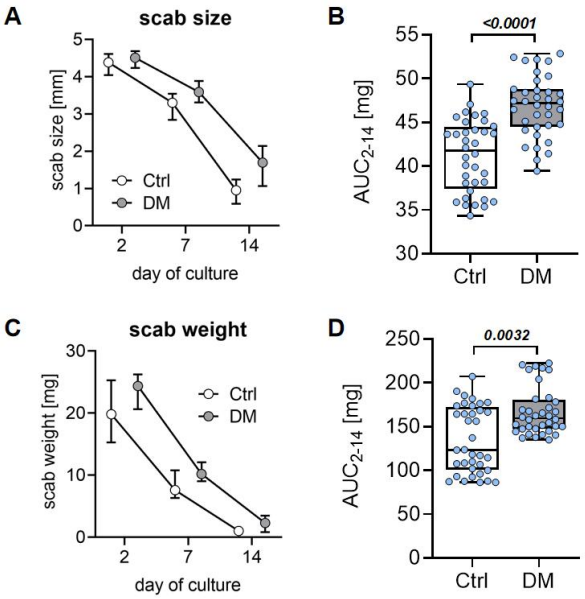


Figure 6: Delayed remodeling in DM scabs. *In vitro* scab models were established using whole blood from non-diabetic control (Ctrl, N = 6) and diabetic (DM, N = 6) patients. (A) Dynamic changes in scab diameter over 14 days of culture. (B) Quantification of AUC for scab size from Day 2 to Day 14. (C) Dynamic changes in scab weight over the culture period. (D) AUC analysis of scab weight from Day 2 to Day 14. Statistical significance was determined by the Mann-Whitney test.

3.2. Dysregulated EMT in DM scabs

3.2.1. Enhanced expression of epithelial markers in DM scabs

To examine the molecular foundation of delayed scab remodeling in DM, we evaluated the expression of critical EMT genes by quantitative PCR. Representative gel images at various time intervals (days 2, 7, and 14) demonstrated consistently elevated levels of epithelial markers in the DM group (Figure 7A). The quantification of net AUC values demonstrated a significant upregulation of *E-cadherin* ($p < 0.001$) (Figure 7B), signifying

persistent epithelial traits. Notable overexpression was also detected for epithelial keratins, specifically *Keratin 18* ($p = 0.003$) (Figure 7C) and *Keratin 19* ($p < 0.001$) (Figure 7D), in addition to *Syndecan 1* ($p = 0.0009$) (Figure 7E), thereby reinforcing this finding. The sustained elevated expression of these epithelial markers indicates that scabs from diabetic patients do not undergo timely EMT, hence contributing to impaired remodeling.

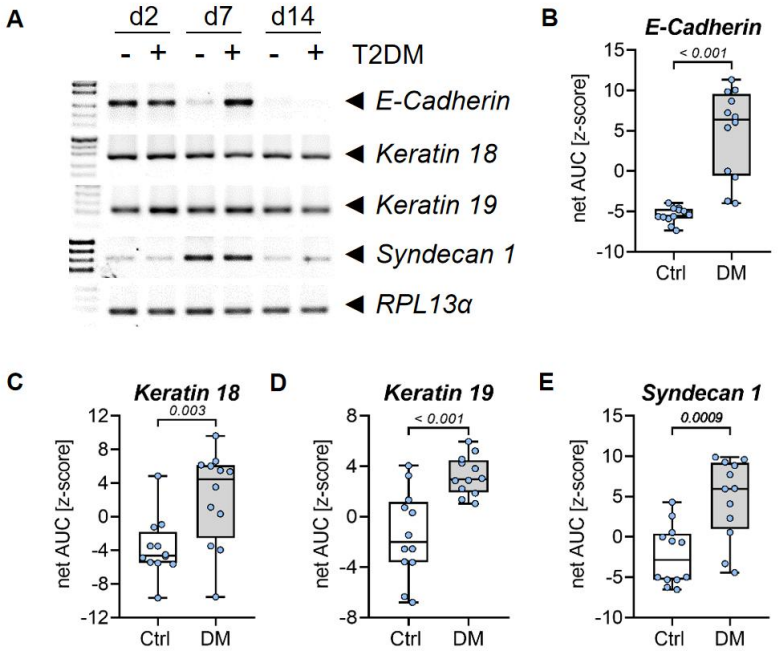


Figure 7: Compared to control scabs, DM scabs show enhanced expression of epithelial markers. Semiquantitative PCR analysis of epithelial cell-adhesion markers in scabs from Ctrl and DM patients over Day 2 – Day 14 culture period. (A) Representative gel images showing expression of *E-cadherin*, *Keratin 18*, *Keratin 19*, *Syndecan 1*, and *RPL13α* (loading control) at days 2, 7, and 14. -, Ctrl; +, DM. Net AUC (z-score) was calculated for each gene. (B) *E-cadherin* expression. (C) *Keratin 18* expression. (D) *Keratin 19* expression. (E) *Syndecan 1* expression. N = 3; n = 4. Statistical significance was determined by Mann-Whitney U test.

3.2.2. Low expression of mesenchymal markers in DM scabs

Consistent with the observed epithelial features, representative gel images across different time points (day 2, 7, and 14) revealed altered expression patterns of mesenchymal markers in DM scabs (Figure 8A). Quantification showed that expression of the key mesenchymal marker *N-cadherin* was significantly reduced in DM scabs compared with Ctrl scabs ($p = 0.004$) (Figure 8B). Although *Vimentin* expression did not show significant changes ($p = 0.410$)

(Figure 8C) between Ctrl and DM scabs, both *Fibronectin* (p = 0.078) (Figure 8D) and *Collagen type I alpha 1* (*COL1A1*; p = 0.060) (Figure 8E) demonstrated declining trends, further indicating inadequate mesenchymal transition in DM scabs.

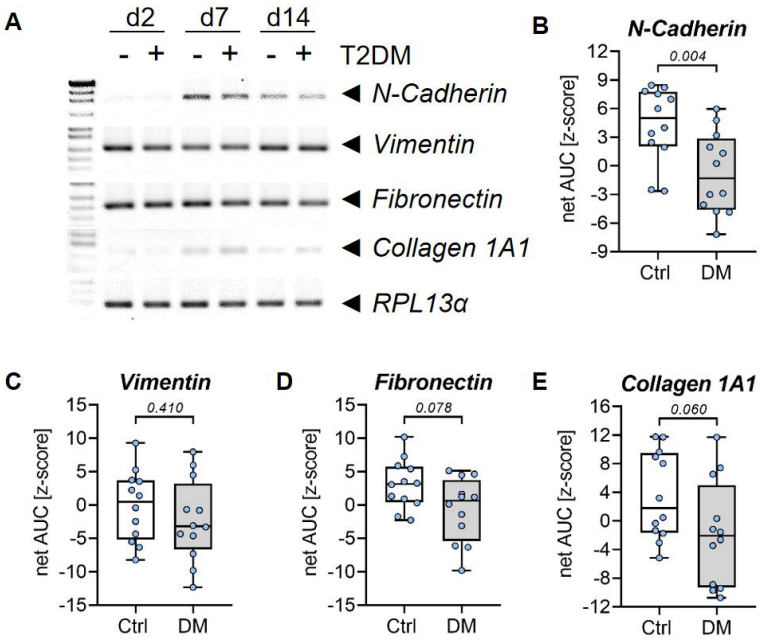


Figure 8: Compared to control scabs, DM scabs show lower expression of mesenchymal markers. Semiquantitative PCR analysis of mesenchymal markers in scabs from Ctrl and DM patients over Day 2 – Day 14 culture period. (A) Representative gel images showing expression of *N-cadherin*, *Vimentin*, *Fibronectin*, *Collagen 1A1*, and *RPL13α* (loading control) at days 2, 7, and 14. -, control; +, DM. Net AUC (z-score) was calculated for each gene. (B) *N-cadherin* expression. (C) *Vimentin* expression. (D) *Fibronectin* expression. (E) *COL1A1* expression. N = 3; n = 4. Statistical significance was determined by Mann-Whitney U test.

3.2.3. Expression of EMT transcription factors is affected in DM scabs

The evaluation of the primary transcription factors regulating EMT indicated a complicated pattern of dysregulated expression. Representative gel images at various time intervals (day 2, 7, and 14) showed altered expression patterns of EMT transcription factors in DM scabs (Figure 9A). Quantification revealed that *Snail1* showed only a non-significant trend toward increased expression (p = 0.068) (Figure 9B). In contrast, two key EMT transcription factors, *Snail2* (p = 0.039) (Figure 9C) and *ZEB1* (p = 0.024) (Figure 9D), were significantly upregulated in DM scabs. Contrarily, *ZEB2*, another critical EMT regulator, was significantly downregulated (p = 0.033) (Figure 9E), suggesting distinct

regulatory pathways. Collectively, this molecular signature, characterized by persistently elevated epithelial markers, reduced *N-cadherin* expression, and imbalanced transcription factor results, strongly supports impaired EMT, which likely underlies delayed scab remodeling in diabetic conditions.

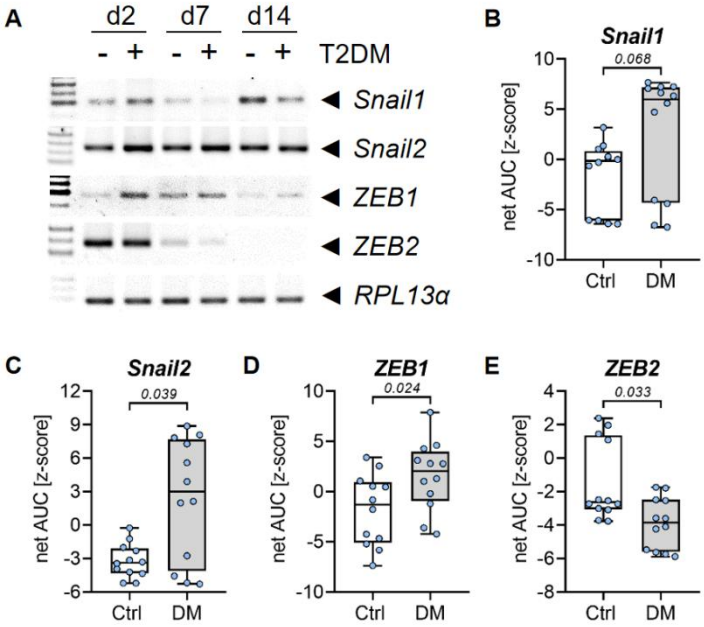


Figure 9: Dysregulated expression of EMT transcription factors in DM scabs. Semiquantitative PCR analysis of EMT-regulating transcription factors in scabs from Ctrl and DM patients over the Day 2 – Day 14 culture period. (A) Representative gel images showing expression of *Snail1*, *Snail2*, *ZEB1*, *ZEB2*, and *RPL13α* (loading control) at days 2, 7, and 14. -, Ctrl; +, DM. Net AUC (z-score) was calculated for each gene. (B) *Snail1* expression. (C) *Snail2* expression. (D) *ZEB1* expression. (E) *ZEB2* expression. N = 3; n = 4. Statistical significance was determined by Mann-Whitney U test.

3.2.4. Assessment of matrix metalloproteinases (MMPs) and inhibitor expression

Based on the observed impairment in scab remodeling, we further evaluated the expression of genes associated with ECM degradation. Representative gel images analysis across different time points (day 2, 7, and 14) showed expression patterns of matrix metalloproteinases and their inhibitors in DM and Ctrl scabs (Figure 10A). The expression of matrix metalloproteinases (*MMP1*, *MMP2*, and *MMP9*) and their respective tissue inhibitors of metalloproteinases (*TIMP1* and *TIMP2*) was assessed over the 14-day culture period. Quantification revealed no statistically significant differences between DM

scabs and Ctrl scabs for any of the tested MMP genes: *MMP1* (p = 0.1782) (Figure 10B), *MMP2* (p = 0.3696) (Figure 10C), and *MMP9* (p = 0.1600) (Figure 10D). Similarly, no significant differences were observed for the tissue inhibitors *TIMP1* (p = 0.1782) (Figure 10E) and *TIMP2* (p = 0.7553) (Figure 10F). These findings suggest that the delayed remodeling in diabetic scabs is primarily linked to dysregulation of the cellular EMT process rather than alterations in these specific ECM-regulatory genes.

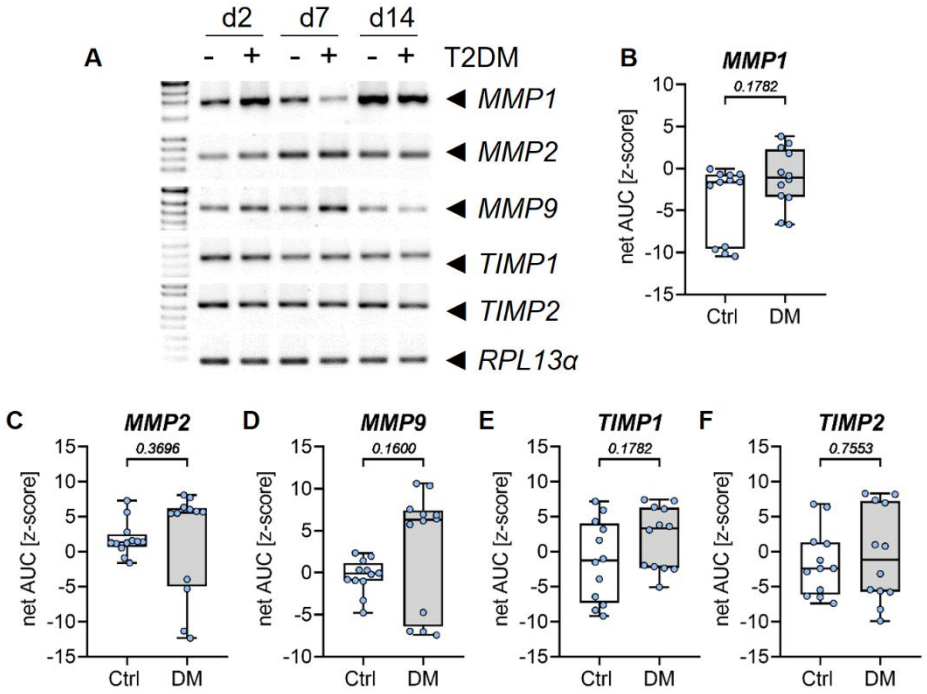


Figure 10: Expression of *MMP1*, *MMP2*, *MMP9*, *TIMP1* and *TIMP2* in scabs. Semiquantitative PCR analysis of ECM degradation-associated genes in scabs from Ctrl and DM patients over Day 2 – Day 14 culture period. (A) Representative gel images showing expression of *MMP1*, *MMP2*, *MMP9*, *TIMP1*, *TIMP2*, and *RPL13α* (loading control) at days 2, 7, and 14. -, control; +, DM. Net AUC (z-score) was calculated for each gene. (B) *MMP1* expression. (C) *MMP2* expression. (D) *MMP9* expression. (E) *TIMP1* expression. (F) *TIMP2* expression. N = 3; n = 4. Statistical significance was determined by Mann-Whitney U test.

3.3. Study cohort characterization

3.3.1. Increased expression of DPP4 in DM scabs

To further examine the molecular pathways contributing to defective remodeling, we evaluated the expression of the glucose metabolism-related enzyme DPP4 in *in vitro* scabs over the Day 2–Day 14 culture period. The

expression of *DPP4* was significantly increased in DM-derived scabs compared with Ctrl scabs (p = 0.0029) (Figure 11A).

3.3.2. Systemic upregulation of DPP4 in Pre-DM and DM patients

The baseline characteristics of the study population is given in Table 8.

Table 8: Baseline characteristics of patients (ELISA)

Variable	Control	Pre-diabetes	Diabetes	p-value
HbA1c (%)	5.3 [5.1, 5.4]	5.9 [5.9, 6.1]	6.9 [6.1, 7.8]	<0.0001
Sex				0.3061
Female	22 (52.4%)	15 (35.7%)	18 (43.9%)	
Male	20 (47.6%)	27 (64.3%)	23 (56.1%)	
Age (years)	64 [58, 68]	63 [61, 68]	64 [58, 68]	0,7940
Waist Circum. (cm)	96.13 ± 18.99	102.97 ± 15.48	112.70 ± 15.13	<0.0001
Height (cm)	168 [159, 178]	168 [157, 178]	169 [161, 178]	0.9812
Weight (kg)	81.64 ± 18.38	89.05 ± 17.29	95.20 ± 19.39	0.0009
BMI	26.9 [23.2, 30.8]	28.8 [25.3, 33.1]	31.6 [27.9, 35.1]	0.0021
FINDRISK	10 [7, 13]	13 [8, 16]	18 [14, 25]	<0.0001
Alcohol Consumption				0.3010
Daily	6 (14.3%)	4 (9.5%)	7 (17.1%)	
>1 / week	15 (35.7%)	11 (26.2%)	7 (17.1%)	
Never/Rarely	18 (42.9%)	26 (61.9%)	26 (63.4%)	
>1 / Day	3 (7.1%)	1 (2.4%)	1 (2.4%)	
Smoking				0.0003
Active smoker	4 (9.5%)	11 (26.2%)	6 (14.6%)	
Ex-smoker	12 (28.6%)	14 (33.3%)	27 (65.9%)	
Non-Smoker	26 (61.9%)	17 (40.5%)	8 (19.5%)	
Years since quitting	0 [0, 9]	0 [0, 9]	13 [0, 30]	0.0024
Packyears	0.0 [0.0, 7.5]	3.0 [0.0, 20.0]	15.0 [3.0, 35.0]	0.0002
Leukocytes	6.29 ± 1.29	7.13 ± 2.06	7.89 ± 2.05	0.0001
Lymphocytes	5.46 [1.98, 6.20]	5.46 [2.60, 7.16]	6.49 [1.73, 8.46]	0.1906
Erythrocytes	4.44 ± 0.70	4.72 ± 0.52	4.66 ± 0.49	0.0891
Hemoglobin	13.62 ± 1.84	14.07 ± 1.42	13.90 ± 1.42	0.4097
MCH	30.7 [29.7, 31.7]	30.4 [29.0, 31.2]	30.0 [28.7, 31.2]	0.0876
MCHC	34.0 ± 1.1	33.4 ± 1.1	33.3 ± 1.1	0.0031
MCV	90.1 [86.8, 92.4]	90.1 [86.9, 93.3]	89.1 [87.0, 91.6]	0.8343
Thrombocytes	241.74 ± 69.03	257.40 ± 55.03	269.20 ± 72.59	0.0590
MTV	10.00 ± 1.16	9.96 ± 0.86	10.03 ± 1.12	0.8680
APTT	24 [23, 25]	24 [22, 25]	23 [22, 24]	0.0858
QUICK (%)	102 [97, 112]	107 [99, 115]	105 [95, 114]	0.7038
C-reactive protein	2.20 [0.73, 5.85]	2.20 [1.10, 6.68]	4.50 [1.00, 9.20]	0.4674
Creatinine	0.80 [0.72, 1.00]	0.90 [0.70, 1.10]	0.80 [0.70, 1.00]	0.5210

Data are presented as mean ± standard deviation (SD) for normally distributed variables, median [IQR] for non-normally distributed variables, and frequency (%) for categorical variables. Group differences were assessed using one-way ANOVA (parametric) or the Kruskal-Wallis test (non-parametric) for continuous data. Categorical variables were compared using the Chi-square test or Fisher's exact test when the expected cell count was less than 5.

Furthermore, ELISA analysis demonstrated that serum DPP4 levels were significantly elevated in both Pre-DM group (p = 0.0033) and T2DM group (p = 0.0005) groups relative to Ctrl group (N = 42 per group) (Figure 11B). These findings suggest that systemic elevation of DPP4 in diabetic patients may contribute to the observed local impairment of scab remodeling and EMT processes.

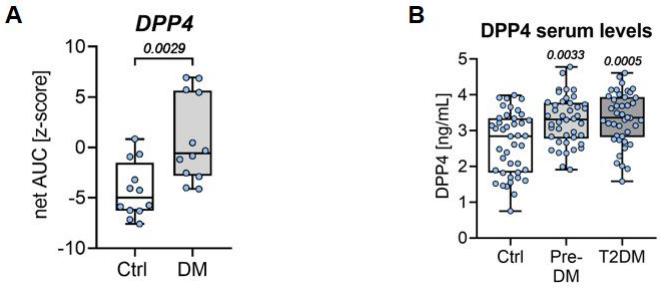


Figure 11: Systemic and local upregulation of DPP4 in DM. (A) Semiquantitative PCR analysis of *DPP4* gene expression in scabs from Ctrl and DM patients over Day 2–Day 14 culture period. Net AUC (z-score) was calculated for *DPP4* gene. (B) serum DPP4 protein levels in control (Ctrl, N = 42), pre-diabetic (Pre-DM, N = 42), and type 2 diabetic (T2DM, N = 42) patients were determined by ELISA. Statistical significance was determined by Mann-Whitney U test.

3.3.3. Clinical characteristics of the study cohort

Patients were categorized into Ctrl, Pre-DM, and T2DM groups based on clinical diagnosis and established glycosylated hemoglobin A1c (HbA1c) thresholds (Ctrl: <5.7%; Pre-DM: 5.7–6.3%; T2DM: ≥6.4%). Analysis of key clinical anthropometric parameters revealed significant differences among the groups (Figure 12). The T2DM group exhibited significantly higher body mass index (BMI) compared with the Ctrl group (p = 0.0012) (Figure 12A), accompanied by a marked increase in waist circumference (p < 0.0001) (Figure 12B), indicating greater prevalence of metabolic syndrome features in the diabetic cohorts. Donor age was comparable across all groups (p > 0.05) (Figure 12C), and variables such as sex (Figure 12D), alcohol consumption

(Figure 12E), and smoking status (Figure 12F) were balanced among the three cohorts (n = 42 per group).

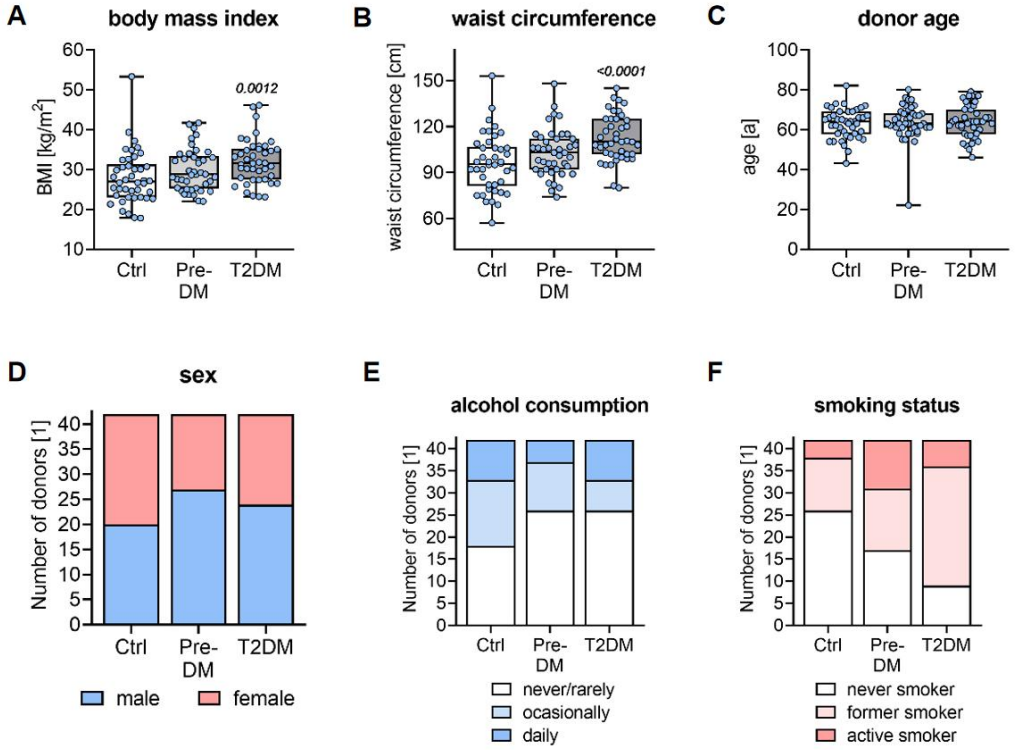


Figure 5: Clinical anthropometric characteristics of the study cohort. Clinical parameters were assessed in control (Ctrl, N = 42), pre-diabetic (Pre-DM, N = 42), and type 2 diabetic (T2DM, N = 42) patients. (A) BMI. (B) Waist circumference. (C) Donor age. (D) sex. (E) alcohol consumption. (F) smoking status. Statistical significance was determined by Kruskal-Wallis test for A, B, C, p-values as compared to Ctrl Group.

3.3.4. Hematological characteristics of the study cohort

Hematological analysis showed that leukocyte counts were significantly elevated in the T2DM group relative to the Ctrl group (p = 0.0003) (Figure 13A), with a similar trend observed in the Pre-DM group (p = 0.0618). Lymphocyte counts also tended to be higher in the T2DM group (p = 0.0942) (Figure 13B). In contrast, mean corpuscular hemoglobin concentration (MCHC) was significantly reduced in the T2DM group (p = 0.0099) (Figure 13E). No significant differences were observed among the three cohorts for erythrocyte count (Figure 13C), platelet count (Figure 13D), mean corpuscular volume (MCV) (Figure 13F), mean corpuscular hemoglobin (MCH) (Figure 13G), or hemoglobin (Figure 13H).

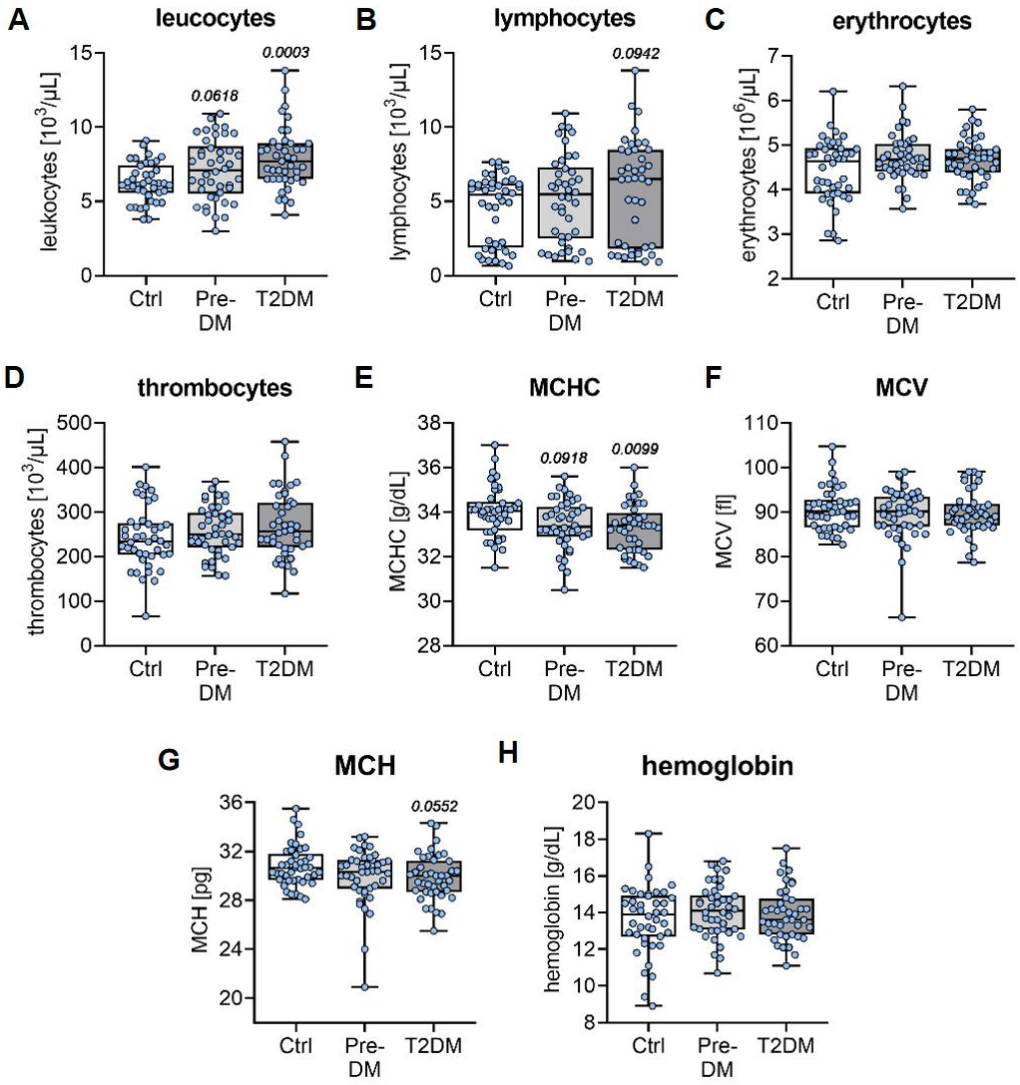


Figure 6: Hematological characteristics of the study cohort. Hematological parameters were assessed in control (Ctrl, N = 42), pre-diabetic (Pre-DM, N = 42), and type 2 diabetic (T2DM, N = 42) patients. (A) leukocyte counts. (B) lymphocyte counts. (C) erythrocyte counts. (D) thrombocyte counts. (E) MCHC levels. (F) MCV levels. (G) MCH levels. (H) hemoglobin levels. Statistical significance was determined by Kruskal-Wallis test. P-values as compared to Ctrl Group.

3.4. Addition of exogenous DPP4 impaired scab remodeling

To assess the function of DPP4 in the *in vitro* scab remodeling, recombinant human DPP4 (rhDPP4, 500 ng/ml) and the specific DPP4 inhibitor sitagliptin (DPP4i, 400 ng/ml) were added to the culture medium of scabs. Exogenous rhDPP4 treatment significantly impaired scab remodeling, as evidenced by delayed reduction in scab size (Figure 14A) and scab weight (Figure 14B) compared with untreated Ctrl. This impairment was quantitatively reflected by

a marked increase in the AUC for both scab size ($p < 0.001$) (Figure 14C) and scab weight ($p < 0.01$) (Figure 14D). In contrast, treatment with DPP4i substantially accelerated the remodeling process. Specifically, compared with the rhDPP4-treated group, DPP4i treatment resulted in significantly reduced AUC values for scab size ($p < 0.05$) and scab weight ($p < 0.05$). Notably, DPP4i treatment even promoted faster remodeling than in untreated Ctrl ($p < 0.05$ for size; $p < 0.05$ for weight). The findings indicate that elevated DPP4 activity may cause a detrimental delay in scab remodeling, whereas its pharmacological suppression can facilitate and enhance the remodeling process.

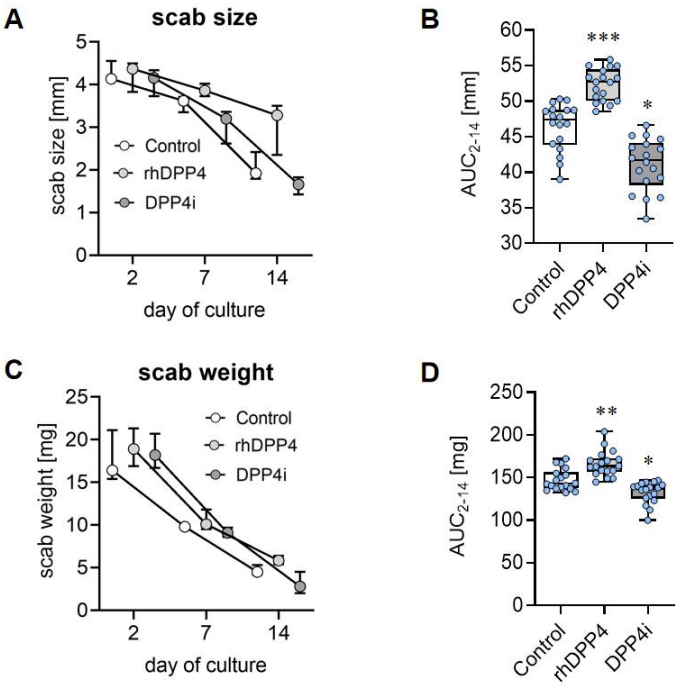


Figure 7: Modulation of DPP4 activity alters scab remodeling kinetics in control scabs. Control scabs were treated with rhDPP4, DPP4i. (A) Scab size dynamics over 14 days and (B) AUC quantification. (C) Scab weight dynamics and (D) AUC quantification. N = 3 independent experiments; n = 6 per group. Statistical significance was determined by Kruskal-Wallis test with post-hoc comparisons. *p < 0.05, **p < 0.01, ***p < 0.001 as compared to Ctrl group.

3.5. BBR inhibits DPP4 and promotes scab remodeling

3.5.1. Pharmacological validation of BBR as a DPP4 inhibitor

Considering the critical function of DPP4 activity in delayed scab remodeling, we aimed to identify a clinically pertinent drug that may pharmacologically

inhibit this enzyme. We identified BBR, a natural isoquinoline alkaloid recognized for its anti-diabetic and anti-inflammatory attributes, as a viable option. A DPP4 activity experiment shown that BBR significantly inhibits DPP4 activity in a dose-dependent manner (Figure 15). The dose-response analysis revealed that the half-maximal inhibitory concentration (IC50) of BBR for DPP4 activity is approximately 30 µM. A concentration of 100 µM BBR reached DPP4 inhibition comparable to that of the synthetic positive control, sitagliptin (400 ng/mL) (Figure 15). These results confirm BBR as a natural, clinically relevant DPP4 inhibitor.

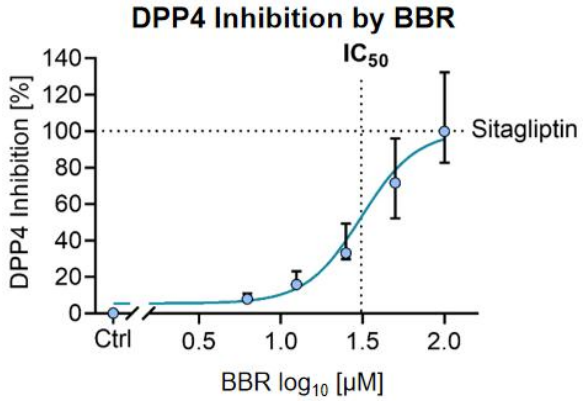


Figure 8: Dose-dependent inhibition of DPP4 activity by BBR. DPP4 enzymatic activity was measured in the presence of increasing concentrations of BBR (log10 scale). Sitagliptin (positive control) achieved complete inhibition (100%) at the tested concentration. Data are presented as median ± 95%-CI from three independent experiments.

3.5.2. Cytotoxicity assessment of BBR with scabs

Prior to evaluating its therapeutic effects, we assessed the cytotoxicity of BBR on *in vitro* scabs to establish a safe therapeutic window. Scabs were cultured with BBR at concentrations ranging from 6.25 µM to 100 µM for up to 14 days (Figure 16A-B). Mitochondrial activity, quantified by the resazurin conversion assay, indicated that BBR at concentrations up to 100 µM did not exhibit statistically significant cytotoxicity compared with untreated controls (0 µM) at Day 2, Day 7, or Day 14 (Figure 16A). Morphological assessment via Calcein-AM staining corroborated these findings, demonstrating preserved cell viability and intact cellular architecture across all tested concentrations and time points (Figure 16B). These results confirm that BBR is safe for further

functional assays at concentrations up to 100 µM.

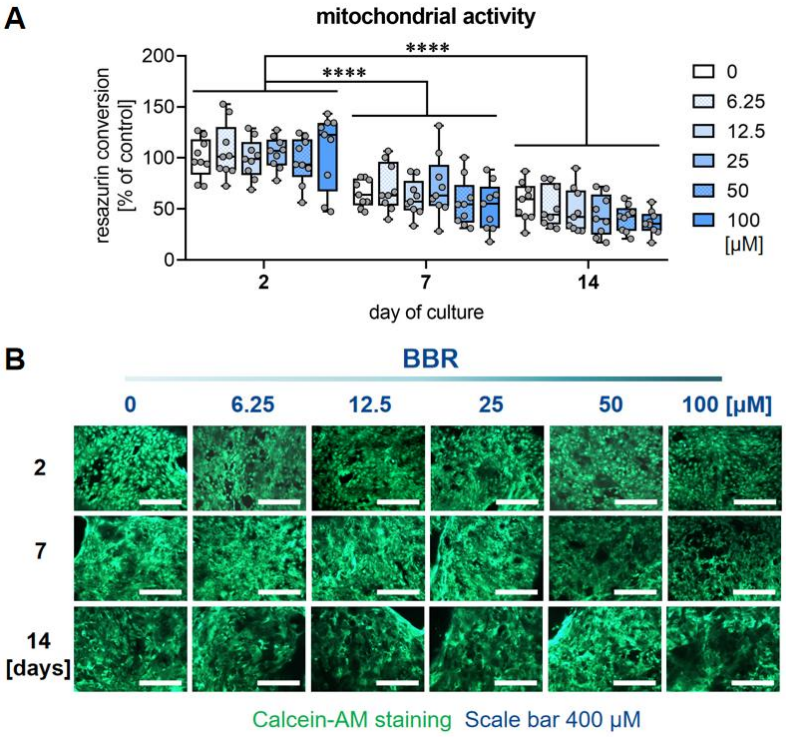


Figure 9: Cytotoxicity assessment of BBR in *in vitro* scabs. (A) Mitochondrial activity measured by resazurin conversion assay in scabs treated with increasing concentrations of BBR (0, 6.25, 12.5, 25, 50, and 100 µM) at Day 2, Day 7, and Day 14. (Dunnett's multiple comparisons test; ****$p < 0.0001$; $N = 3$, $n \geq 3$). Data are presented as percentage of control. (B) Representative Calcein-AM staining images. Scale bar, 400 µm.

3.5.3. BBR restores remodeling dynamics in DM scabs

Based on its DPP4 inhibitory activity and confirmed safety range, we evaluated the ability of BBR to restore impaired remodeling in DM-derived scabs (Figure 17). DM scabs were treated with 50 µM or 100 µM BBR for 14 days. Following treatment, scab remodeling was significantly accelerated, resulting in markedly reduced final scab size (Figure 17A) and lower weight (Figure 17C) compared with untreated DM scabs (0 µM). The quantitative study of the remodeling process by AUC validated the therapeutic efficacy of BBR. The 50 µM BBR therapy notably reduced the AUC of scab size and scab weight in comparison to the DM control group (Figure 17B, D). These findings indicate that BBR, through its DPP4 inhibiting mechanism, dose-dependently alleviates the delayed remodeling associated with DM scabs.

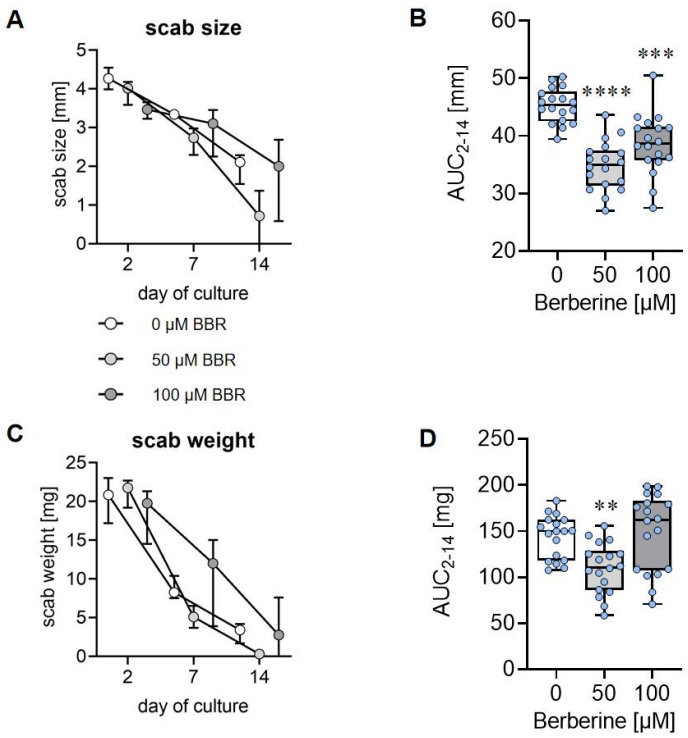


Figure 10: BBR restores remodeling dynamics in diabetic scabs. DM scabs were treated with BBR (0, 50, or 100 µM) for 14 days. (A) Dynamic changes in scab diameter over the culture period. (B) AUC analysis of scab size (Day 2–14). (C) Dynamic changes in scab weight over the culture period. (D) AUC analysis of scab weight. N = 3; n = 6. Statistical significance was determined by Kruskal-Wallis test. **p < 0.01, ***p < 0.001, ****p < 0.0001 vs 0 µM BBR.

3.6. BBR effects on EMT in DM scabs

3.6.1. BBR lowers DPP4 and epithelial marker expression in DM scabs

To determine whether BBR-induced acceleration of remodeling involves EMT, we performed gene expression analysis on DM scabs treated with BBR (0, 50, or 100 µM) and harvested on Day 2 (Figure 18). Representative gel images analysis demonstrated dose-dependent effects of BBR on EMT-related gene expression (Figure 18A). In accordance with its role as a DPP4 inhibitor, BBR treatment resulted in a dose-dependent downregulation of the target gene *DPP4* (50 µM: $p < 0.01$; 100 µM: $p < 0.0001$) (Figure 18B). The decrease in *DPP4* expression was associated with a distinct reversal of the elevated epithelial signature typical of diabetic scabs. Expression of *E-cadherin* was significantly decreased following BBR treatment (100 µM: $p < 0.0001$) (Figure 18C). Similarly, *Keratin 18* and *Keratin 19* exhibited significant,

dose-dependent downregulation (*Keratin 18* at 100 µM: $p < 0.01$; *Keratin 19* at 100 µM: $p < 0.0001$) (Figure 18D-E). These findings indicate that BBR effectively suppresses the persistent epithelial phenotype at the gene expression level, therefore reinstating EMT processes.

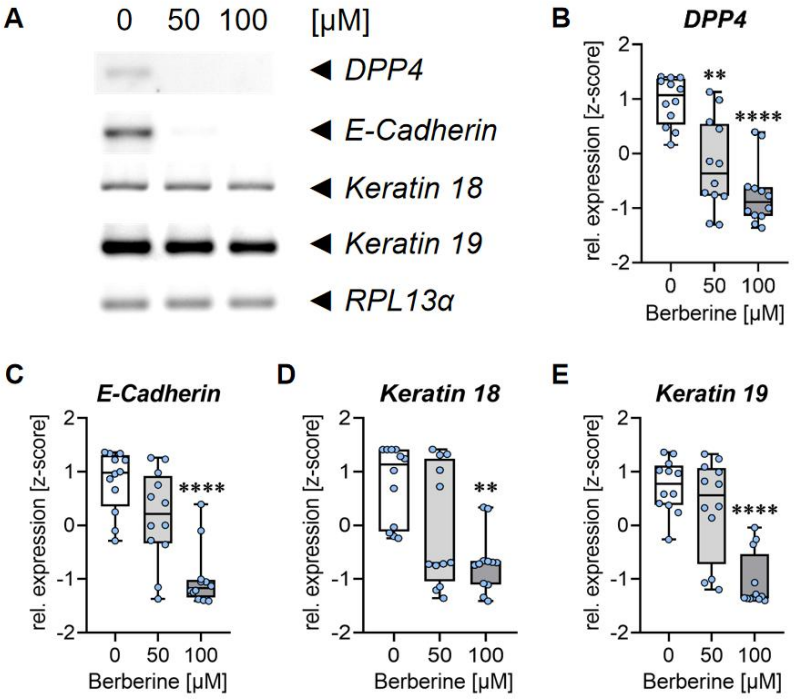


Figure 11: BBR attenuates *DPP4* and epithelial marker expression in DM scabs. Semiquantitative PCR analysis of gene expression in DM scabs treated with BBR (0, 50, or 100 µM) on Day 2. (A) Representative gel images showing expression of *DPP4*, *E-cadherin*, *Keratin 18*, *Keratin 19*, and *RPL13α* (loading control) at different BBR concentrations. Relative expression (z-score) is shown for (B) *DPP4*, (C) *E-cadherin*, (D) *Keratin 18*, and (E) *Keratin 19*. Statistical significance was determined by Kruskal-Wallis test. **p < 0.01, ****p < 0.0001 vs 0 µM BBR.

3.6.2. BBR induces expression of mesenchymal markers in DM scabs

Concurrent with the reduction of epithelial markers, we tested the expression of key mesenchymal markers in DM scabs (Figure 19). Representative gel images analysis demonstrated dose-dependent effects of BBR on mesenchymal marker expression (Figure 19A). *N-cadherin*, previously downregulated in diabetic scabs, was significantly and dose-dependently restored by BBR (50 µM: $p < 0.05$; 100 µM: $p < 0.01$) (Figure 19B). In addition, *Fibronectin*, another critical mesenchymal extracellular matrix component, was significantly upregulated at the highest BBR concentration (100 µM: $p < 0.05$)

(Figure 19D). *Vimentin* exhibited an upward trend, though it did not reach statistical significance (Figure 19C). This coordinated regulation confirms that BBR effectively promotes the transition toward a mesenchymal phenotype.

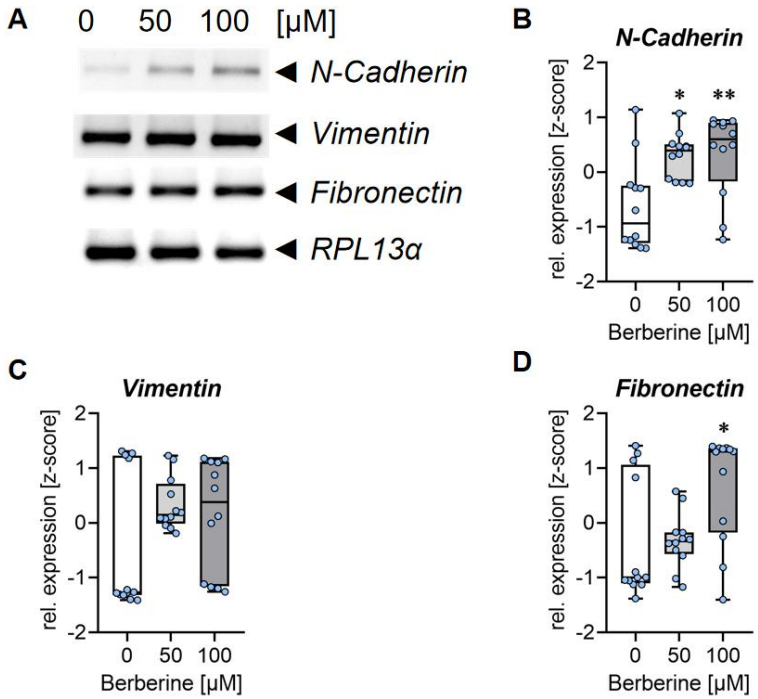


Figure 12: BBR induces pro-mesenchymal marker expression in diabetic scabs. Semiquantitative PCR analysis of mesenchymal markers in DM scabs treated with BBR (0, 50, or 100 µM) on Day 2. (A) Representative gel images showing expression of *N-cadherin*, *Vimentin*, *Fibronectin*, and *RPL13α* (loading control) at different BBR concentrations. Relative expression (z-score) is shown for (B) *N-cadherin*, (C) *Vimentin*, and (D) *Fibronectin*. Statistical significance was determined by Kruskal-Wallis test. *$p < 0.05$, **$p < 0.01$ vs 0 µM BBR.

3.6.3. BBR normalizes key EMT transcription factors in DM scabs

To determine whether BBR intervention could reverse the dysregulated EMT transcriptional program, we lastly analyzed key EMT-regulating transcription factors (Figure 20). Representative gel images analysis demonstrated dose-dependent effects of BBR on EMT transcription factor expression (Figure 20A). BBR dose-dependently induced the expression of *Snail1* and *ZEB1* (*Snail1* at 50 µM and 100 µM: $p < 0.0001$; *ZEB1* at 100 µM: $p < 0.05$) (Figure 20B, D). Simultaneously, expression of *Snail2* (100 µM: $p < 0.0001$) and *ZEB2* (50 µM: $p < 0.01$; 100 µM: $p < 0.0001$) was markedly suppressed (Figure 20C, E). The resultant signature, characterized by reduced epithelial markers,

enhanced mesenchymal markers, and transcription factor shifts that favor EMT progression (high *Snail1/ZEB1* and low *Snail2/ZEB2*), indicates that the DPP4 inhibitory activity of BBR is mechanistically linked to the accelerated remodeling phenotype via regulation of EMT.

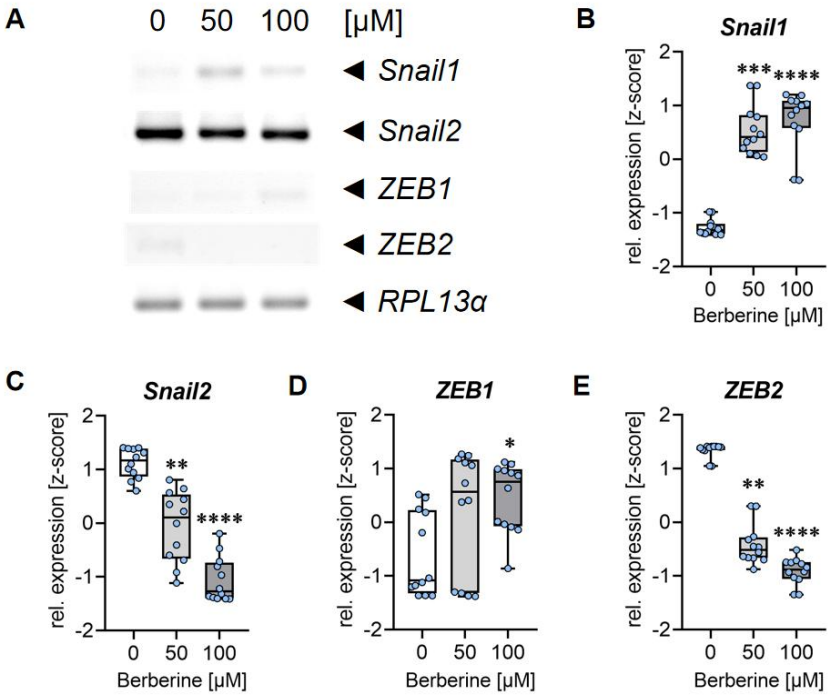


Figure 20: BBR normalizes EMT transcription factor expression in diabetic scabs. Semiquantitative PCR analysis of EMT-regulating transcription factors in DM scabs treated with BBR (0, 50, or 100 µM) on Day 2. (A) Representative gel images showing expression of *Snail1*, *Snail2*, *ZEB1*, *ZEB2*, and *RPL13α* (loading control) at different BBR concentrations. Relative expression (z-score) is shown for (B) *Snail1*, (C) *Snail2*, (D) *ZEB1*, and (E) *ZEB2*. Statistical significance was determined by Kruskal-Wallis test. *p < 0.05, **p < 0.01, ****p < 0.0001 vs 0 µM BBR.

To evaluate whether the observed effects of BBR are specific to the pathological condition of diabetic scabs, parallel experiments were conducted using control scabs. The detailed molecular effects of BBR on gene expression in control scabs, which showed distinct patterns compared to DM scabs, are provided in Appendix A (Figures A1–A3).

4. Discussion

4.1. Impaired scab remodeling in diabetes

Our results clearly demonstrate that scabs derived from diabetic patients exhibit significantly greater size and weight throughout the 14-day *in vitro* culture period. This persistent morphological retention indicates a fundamental defect in the early remodeling capacity of diabetic wounds. This observation aligns with clinical evidence demonstrating delayed wound closure in diabetic patients (Burgess *et al*. 2021). Notably, while previous extensive *in vivo* studies have emphasized that overexpression of MMPs in diabetic foot ulcers accelerates matrix degradation, thereby contributing to impaired wound healing (Lobmann *et al*. 2006, Muller *et al*. 2008), our experimental data reveal no statistically significant differences in mRNA expression of *MMPs* and *TIMPs* between diabetic and control scabs. Meanwhile, the stable expression of TIMP1 and TIMP2 indicates that the diabetic environment does not hinder remodeling through enhanced protease inhibition. This finding carries important clinical implications: for the treatment of early diabetic wounds, simply inhibiting MMPs to reduce tissue degradation may not be the optimal therapeutic strategy.

The divergence between gene expression and morphological changes suggests that the remodeling impairment in diabetic scabs does not stem from insufficient secretion of MMPs and TIMPs, but rather originates from alterations in matrix structural properties. Under hyperglycemic conditions, fibrin within scabs undergoes non-enzymatic glycation, forming stable AGEs. These AGEs enhance the mechanical stiffness of the fibrin meshwork through intermolecular cross-linking, conferring significant protease resistance and thereby suppressing physiological matrix turnover (Lee *et al*. 2019). Furthermore, the persistently higher weight of diabetic scabs indicates impaired cellular-level remodeling function. Under normal conditions, wound healing involves coordinated contraction by myofibroblasts and activated

keratinocytes, generating mechanical forces to reduce wound area (Gabbiani *et al*. 2003). Since the diabetic environment disrupts mechanisms of cellular mechanotransduction, the matrix cannot be effectively contracted and reorganized even with normal MMP levels, resulting in delayed reduction of diabetic scab weight and size.

4.2. Dysregulated EMT as a key mechanism in diabetic wound healing

We found that diabetic scabs exist in a state of partial EMT arrest. Our results showed that *E-cadherin* expression is elevated in the diabetic group, while the upregulation of *N-cadherin* is significantly inhibited. This classic pattern of "maintained epithelial features and blocked mesenchymal traits" suggests that keratinocytes in diabetic patients are restricted to a polarized epithelial state. In the process of physiological healing, keratinocytes must diminish the expression of adhesion junction proteins to attain the phenotypic flexibility required for migration, enabling them to move from the scab's periphery to the center and facilitate diameter retraction (Pastar *et al*. 2014). The continual existence of these sticky structures in the diabetic milieu obstructs this displacement process, establishing the structural foundation for delayed remodeling (Singh *et al*. 2019).

We also identified a dysregulation in the expression of the Snail and ZEB families, which are responsible for the transcriptional control of EMT. Our results show that both *Snail1* and *Snail2* are significantly elevated in the diabetic group, which contradicts the classic understanding of the Snail family’s role in initiating EMT by repressing E-cadherin (Dongre *et al*. 2019). Further analysis suggests that while Snail1 can recruit histone deacetylases to the E-cadherin promoter region, its ability to bind DNA may be compromised in a hyperglycemic microenvironment due to cross-linking alterations caused by advanced glycation end products, resulting in a notable reduction in transcriptional repression efficacy (Khalid *et al*. 2022). The elevation of *Snail2* suggests an imbalance in the critical EMT regulatory network. As an EMT

transcription factor, Snail2 typically works synergistically with ZEB family members to execute the EMT genetic program, promoting cytoskeletal remodeling and the acquisition of motility through complex regulatory networks (Peinado *et al*. 2007). However, the significant downregulation of *ZEB2* in diabetic scabs disrupts this regulatory progression, meaning that despite the activation of upstream migratory signals, the cells remain unable to effectively drive cytoskeletal reorganization and execute migration tasks.

Meanwhile, *ZEB1* is further upregulated in the diabetic group, and its expression is closely linked to intense inflammatory signaling and oxidative stress, primarily inhibiting transcription by binding to E-box sequences on the E-cadherin promoter (Zhang *et al*. 2015). However, ZEB1 activity is more closely associated with the initial induction of mesenchymal markers such as Vimentin and Fibronectin, and it lacks the capacity for precise control over cellular kinetic structures (Zhang *et al*. 2023). In contrast, the downregulation of *ZEB2* may be a central link in healing arrest. ZEB2 not only represses E-cadherin but also positively regulates the dynamic reorganization of basement membrane components (LAMA3 and COL4A1) and induces the polarized distribution of MMP2, which are essential events for directional cell migration within the extracellular matrix (DaSilva-Arnold *et al*. 2019).

The imbalance of microRNA-mediated feedback loops may be another cause of EMT arrest. Research indicates a mutual double-negative feedback loop between the miR-200 family and the ZEB family; metabolic disturbances in the diabetic environment may enhance the inhibitory effect of miR-200 on ZEB2 (Gibbons *et al*. 2009), which aligns with our experimental result that ZEB2 expression is significantly downregulated in diabetic scabs. The collaborative functional deficiency among Snail and ZEB family members underlies the molecular mechanism for impaired wound healing in diabetes.

4.3. DPP4 as a critical regulator of scab remodeling

Our study found that DPP4 expression is significantly increased in both the scab model and the systemic circulation of diabetic patients. Functional validation experiments demonstrated that exogenous rhDPP4 can simulate diabetes-like remodeling delay, while intervention with sitagliptin significantly accelerates the remodeling process. This indicates that DPP4 is not merely a biomarker of diabetes but a factor that directly interferes with wound repair programs (Whittam *et al*. 2019). The observed boosting impact of Sitagliptin in the control group further indicates that physiological levels of DPP4 play a regulatory role in maintaining homeostasis of repair rates. Notably, although systemic DPP4 inhibitors are widely used in clinical diabetes management for glycemic control, their effectiveness in promoting DFU healing remains limited because impaired peripheral circulation and microangiopathy prevent systemic drugs from reaching sufficient concentrations at the ischemic wound site (Marfella *et al*. 2012). DPP4 is a membrane-bound dipeptidase that cleaves two amino acids from the N-terminus of SDF-1α, abolishing its binding activity to the chemokine receptor CXCR4 (Lambeir *et al*. 2003). In addition to SDF-1α, DPP4 can also deactivate neuropeptides associated with wound healing. Substance P and Neuropeptide Y facilitate vasodilation and modulate the recruitment of inflammatory cells during wound formation (Klemann *et al*. 2016). In the diabetic milieu, higher DPP4 activity leads to the fast degradation of neuropeptides, causing prolonged local inflammatory responses at the wound site and concurrently inhibiting matrix protein turnover efficiency (Mulvihill *et al*. 2003).

4.4. BBR as a natural DPP4 inhibitor

Our study identifies BBR as a powerful natural DPP4 inhibitor that can restore diabetic scab remodeling. Our inhibition assays demonstrated that BBR effectively suppresses DPP4 activity with an IC50 of approximately 30 μM, comparable to synthetic inhibitors like Sitagliptin. Simultaneously, cytotoxicity

assessments confirmed that BBR concentrations up to 100 μM do not impair cell viability or mitochondrial activity in the scab model, establishing a reliable therapeutic window for clinical application. The reversal of diabetic remodeling defects by BBR seems to be predominantly facilitated by DPP4 inhibition; BBR treatment diminished the expression of epithelial markers, including *E-cadherin*, while promoting the expression of mesenchymal markers such as *N-cadherin* and *Fibronectin*, ultimately resulting in enhanced scab remodeling function.

Currently, oral BBR faces significant pharmacokinetic limitations that prevent effective delivery to wounds. The absolute oral bioavailability of BBR is less than 1% due to significant first-pass metabolism in the liver and inadequate intestinal membrane permeability (Liu *et al*. 2010). Plasma concentrations after standard oral dosing typically peak at around 10–20 nM (Wang *et al*. 2017), far below the concentrations required for the DPP4 inhibition observed in our study. Even with high-dose regimens or strategies like nanoparticle encapsulation, systemic concentrations rarely exceed 100 nM (Mori *et al*. 2023). Furthermore, the concentration gradient between plasma and wound tissue, coupled with vascular damage in diabetic wounds, prevents oral BBR from reaching therapeutic levels at the wound site (Okonkwo *et al*. 2017). Attempting to overcome this limitation through dose escalation would pose systemic toxicity risks, as high plasma concentrations of BBR can cause gastrointestinal disturbances, elevated liver enzymes, and potential cardiac arrhythmias (Neag *et al*. 2018). Topical application completely bypasses these obstacles; direct application to the wound bed can achieve local concentrations in the micromolar range, maintaining high local activity while minimizing systemic exposure. We observed that 50–100 μM BBR effectively restores diabetic scab remodeling, which is consistent with the concentrations achievable through topical delivery, whereas oral administration could never approach these levels.

Unlike synthetic drugs such as Sitagliptin, BBR possesses multi-target

regulatory properties. In addition to direct DPP4 inhibition, BBR is a potent activator of AMPK (Zhang *et al*. 2008). In the diabetic milieu, persistent high-glucose stress results in mitochondrial malfunction and energy metabolism failure in keratinocytes; EMT, being a highly energy-demanding process, necessitates adequate metabolic support. By activating the AMPK pathway, BBR can optimize cellular energy homeostasis, providing the necessary conditions for the EMT program to proceed (Herzig *et al*. 2018). Furthermore, BBR improves oxidative stress and inflammation levels in diabetic wounds (Panda *et al*. 2021). The accumulation of reactive oxygen species caused by hyperglycemia interferes with the normal function of EMT-related transcription factors (Ko *et al*. 2015). BBR may enhance cellular antioxidant capacity through the activation of the Nrf2 signaling pathway (García-Muñoz *et al*. 2024). BBR is more comprehensive in the treatment of chronic diabetic wounds compared to single-target medications.

4.5. Context-dependent effects and dosing considerations

Our observation that BBR induces different molecular effects in control versus diabetic scabs highlights the context-dependent nature of pharmacological EMT modulation. This differential response, as detailed in the supplementary results (see Appendix A), aligns with previous findings that BBR exhibits distinct regulatory patterns depending on cellular pathological states. BBR has been demonstrated to differentially influence MAPK signaling pathways in normal and diabetes settings, inhibiting Th17 and Th1 cell development through separate mechanisms in type 1 diabetic mice, while displaying varied effects in non-diabetic contexts (Cui *et al*. 2009).

In diabetic scabs, BBR normalized the pathological elevation of epithelial markers and restored mesenchymal marker expression toward healthy levels. In contrast, as shown in Appendix A (Figure A1)**,** BBR treatment in control scabs elevated the expression of *Keratin 18* and *19* while diminishing *E-cadherin*, resulting in a distinct molecular profile compared to diabetic

circumstances.

This context-dependent modulation suggests that BBR regulates cellular plasticity according to the baseline pathological state of the scab. In diabetic conditions where EMT is suppressed, BBR promotes the necessary mesenchymal transition. In normal conditions, BBR may induce a different phenotypic state that reflects enhanced cellular activation rather than simple normalization. Such biphasic or differential effects are consistent with BBR's concentration-dependent actions observed in other systems, where it inhibits cancer cell migration and invasion in a dose-dependent manner while modulating EMT-related genes, including *Snail* and *E-cadherin* (Liu *et al*. 2015).

The dose-dependent effects observed in the control group (Appendix A, Figures A2 and A3) also require careful consideration for clinical application. For instance, in control scabs, BBR at 50 μM downregulated *Snail1*, whereas at 100 μM, it increased this transcription factor; a similar pattern was observed with *ZEB2* expression. This biphasic response indicates complex regulatory mechanisms that may involve different receptor affinities or downstream signaling pathways at varying concentrations. Comparable concentration-dependent dual actions have been documented for BBR in renal tubular epithelial cells, wherein it inhibits EMT via the Notch/Snail pathway at particular concentrations (Liu *et al*. 2024). For clinical application, these findings highlight the importance of optimizing BBR concentrations for specific wound types. Diabetic wounds with elevated baseline DPP4 may necessitate increased dosages to mitigate enzyme elevation, whilst normal wounds may benefit from reduced dosages that facilitate healing without excessive mesenchymal change.

4.6. Limitations of the study

Several limitations should be considered when interpreting our findings. First, the *in vitro* scab model, although useful for studying early wound phases and

blood-keratinocyte interactions, does not capture the full complexity of *in vivo* wound environments. The model does not include fibrocellular interaction, neural input, systemic hormonal regulation, and the complete immune repertoire found in living tissue, all of which could influence healing outcomes.

Secondly, our research predominantly concentrated on alterations in gene expression over a 14-day duration. This timeframe encompasses the initial remodeling phase but excludes the complete maturation process occurring over weeks or months in clinical environments. Subsequent research should prolong the observation duration to assess long-term tissue remodeling, collagen maturation, and scar formation.

Third, while our patient population is thoroughly defined, it reflects a particular demography with type 2 diabetes. Variations in medication history, length of diabetes, glycemic control, and comorbidities such as neuropathy or cardiovascular disease may influence DPP4 levels and treatment responses in manners not entirely encompassed in our research. Furthermore, we did not distinguish between patients with varying diabetes comorbidities, which may independently affect wound healing ability.

Fourth, the study examined gene expression but did not include comprehensive protein-level validation for all markers. Future research should verify that the observed transcriptional changes translate into protein expression alterations using immunohistochemistry.

4.7. Outlook and future directions

Addressing these limitations through translational research will be pivotal. This study substantiates DPP4 as a viable therapeutic target with direct clinical relevance for chronic DFU therapy, where the healing process is often pathologically arrested in the inflammatory phase (Armstrong *et al*. 2017). Current DPP4 inhibitors may be repurposed for wound management. Nonetheless, BBR offers a natural, economical option with reduced adverse effects (Liu *et al*. 2025). BBR has the capability to rehabilitate the impaired

EMT process. Recent research indicated that BBR expedites the healing of diabetic wounds via multiple pathways. The processes encompass the restoration of TrxR1/JNK signaling (Zhou *et al*. 2021), activation of the Nrf2 antioxidant pathway (Zhang *et al*. 2020), and inhibition of IL-17-mediated inflammation (Zhang *et al*. 2022).

Future research should address three key questions. First, *in vivo* studies using diabetic animal models should verify that BBR-mediated DPP4 inhibition accelerates wound healing. Prior research utilizing high-fat diet and streptozotocin-induced diabetic mice demonstrated that BBR and Huangbai liniment, which contains BBR as a principal ingredient, facilitate wound healing. These treatments inhibit IL-17 signaling and reduce downstream inflammatory targets, including CXCL1, CCL2, MMP3, and MMP9 (Zhang *et al*. 2022).

Second, the long-term effects of BBR on scar formation needs to be studied. Excessive EMT promotion may increase fibrosis. Recent evidence shows that BBR-loaded nanofibrous dressings reduce hypertrophic scar formation by inhibiting the TGF-β1/Smad3 pathway (Lv *et al*. 2024). Consequently, BBR may offer dual advantages: expediting wound healing and reducing pathological scarring.

Third, improved BBR delivery systems are crucial for clinical use. Oral BBR has poor pharmacokinetics. Its absolute bioavailability is less than 1% due to hepatic first-pass metabolism and poor intestinal absorption (Panda *et al*. 2021). Innovative delivery mechanisms can address this issue. Lecithin-chitosan nanoparticles enhance local retention of BBR and facilitate prolonged release at wound sites (Panda *et al*. 2021). Electrospun nanofiber dressings using BBR demonstrate favorable outcomes. They expedite wound repair and diminish scar hyperplasia (Lv *et al*. 2024).

Finally, clinical trials are essential. These should compare BBR-based topical therapies with synthetic DPP4 inhibitors. The trials must demonstrate efficacy and safety in people with persistent diabetic ulcers. Histological examination of wound biopsies must also be conducted. This can elucidate EMT regulation in

human wounds.

4.8. Conclusions

In conclusion, this study investigated the molecular mechanisms underlying impaired scab remodeling in diabetic conditions and evaluated BBR as a therapeutic intervention targeting the DPP4-EMT axis.

Our findings validate Hypothesis 1: diabetic conditions significantly impair *in vitro* scab remodeling, as demonstrated by persistently greater scab size and weight throughout the 14-day culture period compared to non-diabetic controls.

Hypothesis 2 was supported by the observation that impaired remodeling is associated with dysregulated EMT, specifically characterized by persistent elevation of epithelial markers (*E-cadherin*, *Keratin 18*, and *Keratin 19*), suppressed expression of the mesenchymal marker *N-cadherin*, and an imbalance in key EMT transcription factors (significantly upregulated *Snail2* and *ZEB1*, and significantly downregulated *ZEB2*).

Hypothesis 3 was confirmed through functional validation experiments: elevated *DPP4* expression and activity constitute a critical molecular mechanism underlying this defect. Exogenous recombinant human DPP4 impaired scab remodeling, whereas pharmacological inhibition with sitagliptin restored normal remodeling dynamics and corrected EMT marker expression.

Finally, Hypothesis 4 was substantiated by demonstrating that BBR, a natural isoquinoline alkaloid, effectively inhibits DPP4 activity with an IC50 of approximately 30 μM. Within a non-cytotoxic range (up to 100 μM), BBR dose-dependently reversed abnormal EMT marker expression, promoted mesenchymal phenotypic transformation, and accelerated scab remodeling in diabetic conditions.

Collectively, these findings establish the DPP4-EMT axis as a promising therapeutic target for chronic diabetic wounds and position BBR as a cost-effective, multi-target natural candidate for local wound treatment, directly

addressing the cell migration defects that underlie delayed healing in diabetes. Considering that the prevalence of diabetes is continuously increasing, and diabetic foot ulcers impose significant economic consequences (Zhou *et al*. 2021), BBR-based treatments may present a possible solution by improving patient outcomes (wound healing) and thus decreasing healthcare expenditures.

5. Summary

Impaired wound healing in diabetic patients exposes a great clinical and economic burden to the health care systems. This study aimed to investigate the effect of Berberine (BBR), a natural DPP4 inhibitor, on diabetic wound remodeling *in vitro*. Our data demonstrate that diabetic scabs exhibit remodeling impairment due to the stagnation of the EMT process. Specifically, this is manifested by persistently high expression of epithelial markers *E-cadherin*, *Keratin 18*, and *Keratin 19*, suppressed expression of the mesenchymal marker *N-cadherin*, and an imbalance in the expression of key EMT transcription factors: significantly upregulated *Snail2* and *ZEB1*, and significantly downregulated *ZEB2*. We identified DPP4 as a key molecule mediating this defect. Functional validation experiments using recombinant human DPP4 and its specific inhibitor sitagliptin indicate that elevated DPP4 activity is not only a biomarker of diabetes but also a direct cause of impaired wound healing. Pharmacological inhibition of DPP4 can restore normal remodeling dynamics and correct EMT marker expression. Notably, the natural isoquinoline alkaloid BBR effectively inhibits DPP4 activity with an IC50 of approximately 50 μM, and within a non-cytotoxic range (up to 100 μM), it dose-dependently reverses the abnormal expression of EMT markers in diabetic scabs, promotes mesenchymal phenotypic transformation and accelerates scab remodeling. These findings suggest that targeting the DPP4-EMT axis is a promising therapeutic strategy for improving chronic diabetic wounds. As a natural DPP4 inhibitor with multi-target benefits (including AMPK activation and antioxidant effects), BBR provides a cost-effective and safe candidate for local treatment, addressing the underlying cell migration defects that cause delayed healing in diabetic wounds.

6. Zusammenfassung

Gestörte Wundheilung ist eine häufige Komplikation bei Diabetikern. Sie stellt eine erhebliche klinische und wirtschaftliche Belastung für die Gesundheitssysteme dar. Ziel dieser Studie war es, die Wirkung von Berberin (BBR), einem natürlichen DPP4-Inhibitor, auf die Wundregeneration bei Diabetes in vitro zu untersuchen. Unsere Daten zeigen, dass diabetische Wunden aufgrund einer Stagnation des EMT-Prozesses eine gestörte Remodellierung aufweisen. Konkret manifestiert sich dies durch eine persistierend erhöhte Expression der epithelialen Marker *E-Cadherin*, *Keratin 18* und *Keratin 19*, eine unterdrückte Expression des mesenchymalen Markers *N-Cadherin* sowie ein Ungleichgewicht in der Expression von wichtigen EMT-Transkriptionsfaktoren, wobei *Snail2* und *ZEB1* signifikant hochreguliert und *ZEB2* signifikant herunterreguliert sind. Wir identifizierten DPP4 als Schlüsselmolekül, das diesen Defekt vermittelt. Funktionelle Validierungsexperimente unter Verwendung von rekombinantem humanem DPP4 und dessen spezifischem Inhibitor Sitagliptin zeigen, dass eine erhöhte DPP4-Aktivität nicht nur ein Biomarker des Diabetes, sondern auch eine direkte Ursache gestörter Wundheilung darstellt. Die pharmakologische Hemmung von DPP4 kann die normale Remodellierungsdynamik wiederherstellen und die EMT-Markerexpression korrigieren. Bemerkenswerterweise hemmt das natürliche Isochinolin-Alkaloid Berberin (BBR) die DPP4-Aktivität effektiv mit einem IC50 von etwa 50 μM und reversiert innerhalb eines nicht-zytotoxischen Bereichs (bis zu 100 μM) dosisabhängig die abnorme Expression von EMT-Markern in diabetischen Wunden, fördert die Transformation zum mesenchymalen Phänotyp und beschleunigt die Bildung von Extrazellärmatrix. Diese Ergebnisse legen nahe, dass die DPP4-EMT-Achse eine vielversprechende Therapiestrategie zur Verbesserung chronischer diabetischer Wunden darstellt. Als natürlicher DPP4-Inhibitor mit multiplen Targets (einschließlich AMPK-Aktivierung und

antioxidativen Effekten) bietet BBR einen kostengünstigen und sicheren Kandidaten für die lokale Behandlung, der die zugrundeliegenden Zellmigrationsdefekte adressiert, die die verzögerte Heilung diabetischer Wunden verursachen.

7. Bibliography

Ansell DM, Holden KA, Hardman MJ. Animal models of wound repair: Are they cutting it? Exp Dermatol. 2012 Aug;21(8):581-5.

Armstrong DG, Boulton AJM, Bus SA. Diabetic foot ulcers and their recurrence. N Engl J Med. 2017;376(24):2367-2375.

Askari VR, Khosravi K, Baradaran Rahimi V, Garzoli S. A Mechanistic Review on How Berberine Use Combats Diabetes and Related Complications: Molecular, Cellular, and Metabolic Effects. Pharmaceuticals (Basel). 2023 Dec 20;17(1):7.

Bellavite P, Fazio S, Affuso F. A Descriptive Review of the Action Mechanisms of Berberine, Quercetin and Silymarin on Insulin Resistance/Hyperinsulinemia and Cardiovascular Prevention. Molecules. 2023 Jun 1;28(11):4491.

Blanpain C, Fuchs E. Epidermal homeostasis: a balancing act of stem cells in the skin. Nat Rev Mol Cell Biol. 2009 Mar;10(3):207-17.

Boukamp P, Petrussevska RT, Breitkreutz D, Hornung J, Markham A, Fusenig NE. Normal keratinization in a spontaneously immortalized aneuploid human keratinocyte cell line. J Cell Biol. 1988 Mar;106(3):761-71.

Boulton AJ, Vileikyte L, Ragnarson-Tennvall G, Apelqvist J. The global burden of diabetic foot disease. Lancet. 2005 Nov 12;366(9498):1719-24.

Braverman IM. The cutaneous microcirculation. J Investig Dermatol Symp Proc. 2000 Dec;5(1):3-9.

Braverman IM. The cutaneous microcirculation: ultrastructure and microanatomical organization. Microcirculation. 1997 Sep;4(3):329-40.

Burgess JL, Wyant WA, Abdo Abujamra B, Kirsner RS, Jozic I. Diabetic Wound-Healing Science. Medicina (Kaunas). 2021 Oct 8;57(10):1072.

Chen GY, Nuñez G. Sterile inflammation: sensing and reacting to damage. Nat Rev Immunol. 2010 Dec;10(12):826-37.

Cheng HC, Abdel-Ghany M, Pauli BU. A novel consensus motif in fibronectin mediates dipeptidyl peptidase IV adhesion and metastasis. J Biol Chem. 2003 Jul 4;278(27):24600-7.

Chitadze G, Wehkamp U, Janssen O, Brüggemann M, Lettau M. The Serine Protease CD26/DPP4 in Non-Transformed and Malignant T Cells. Cancers (Basel). 2021 Nov 26;13(23):5947.

Cui G, Qin X, Zhang Y, Gong Z, Ge B, Zang YQ. Berberine differentially modulates the activities of ERK, p38 MAPK, and JNK to suppress Th17 and Th1 T cell differentiation in type 1 diabetic mice. J Biol Chem. 2009 Oct 9;284(41):28420-28429.

DaSilva-Arnold SC, Kuo CY, Davra V, Remache Y, Kim PCW, Fisher JP, Zamudio S, Al-Khan A, Birge RB, Illsley NP. ZEB2, a master regulator of the epithelial-mesenchymal transition, mediates trophoblast differentiation. Mol Hum Reprod. 2019 Feb 1;25(2):61-75.

Dong J, Zuo Z, Yan W, Liu W, Zheng Q, Liu X. Berberine ameliorates diabetic

neuropathic pain in a rat model: involvement of oxidative stress, inflammation, and μ-opioid receptors. Naunyn Schmiedebergs Arch Pharmacol. 2019 Sep;392(9):1141-1149.
Dongre A, Weinberg RA. New insights into the mechanisms of epithelial-mesenchymal transition and implications for cancer. Nat Rev Mol Cell Biol. 2019 Feb;20(2):69-84.
Drucker DJ. The biology of incretin hormones. Cell Metab. 2006 Mar;3(3):153-65.
Eming SA, Martin P, Tomic-Canic M. Wound repair and regeneration: mechanisms, signaling, and translation. Sci Transl Med. 2014 Dec 3;6(265):265sr6.
Feng X, Sureda A, Jafari S, Memariani Z, Tewari D, Annunziata G, Barrea L, Hassan STS, Šmejkal K, Malaník M, Sychrová A, Barreca D, Ziberna L, Mahomoodally MF, Zengin G, Xu S, Nabavi SM, Shen AZ. Berberine in Cardiovascular and Metabolic Diseases: From Mechanisms to Therapeutics. Theranostics. 2019 Mar 16;9(7):1923-1951.
Gabbiani, G. (2003). "The myofibroblast in wound healing and fibrocontractive diseases." J Pathol 200(4): 500-503.
Gaggini M, Sabatino L, Suman AF, Chatzianagnostou K, Vassalle C. Insights into the Roles of GLP-1, DPP-4, and SGLT2 at the Crossroads of Cardiovascular, Renal, and Metabolic Pathophysiology. Cells. 2025 Mar 6;14(5):387.
Gallagher KA, Liu ZJ, Xiao M, Chen H, Goldstein LJ, Buerk DG, Nedeau A, Thom SR, Velazquez OC. Diabetic impairments in NO-mediated endothelial progenitor cell mobilization and homing are reversed by hyperoxia and SDF-1 alpha. J Clin Invest. 2007 May;117(5):1249-59.
Gao W, Chen D, He H, Jiang N, Chen L, Ran X. Sitagliptin, a DPP-4 Inhibitor, Effectively Promotes the Healing of Diabetic Foot Ulcer: A Randomized Controlled Trial. J Diabetes. 2025 Sep;17(9):e70156.
García-Muñoz AM, Victoria-Montesinos D, Ballester P, Cerdá B, Zafrilla P. A Descriptive Review of the Antioxidant Effects and Mechanisms of Action of Berberine and Silymarin. Molecules. 2024 Sep 26;29(19):4576.
Giacco F, Brownlee M. Oxidative stress and diabetic complications. Circ Res. 2010;107(9):1058-1070.
Gibbons DL, Lin W, Creighton CJ, Rizvi ZH, Gregory PA, Goodall GJ, Thilaganathan N, Du L, Zhang Y, Pertsemlidis A, Kurie JM. Contextual extracellular cues promote tumor cell EMT and metastasis by regulating miR-200 family expression. Genes Dev. 2009 Sep 15;23(18):2140-51.
Hayden MS, Ghosh S. Shared principles in NF-kappaB signaling. Cell. 2008 Feb 8;132(3):344-62.
Heher P, Mühleder S, Mittermayr R, Redl H, Slezak P. Fibrin-based delivery strategies for acute and chronic wound healing. Adv Drug Deliv Rev. 2018 Apr;129:134-147.
Herzig S, Shaw RJ. AMPK: guardian of metabolism and mitochondrial

homeostasis. Nat Rev Mol Cell Biol. 2018 Feb;19(2):121-135.
Hinchliffe RJ, Valk GD, Apelqvist J, Armstrong DG, Bakker K, Game FL, Hartemann-Heurtier A, Löndahl M, Price PE, van Houtum WH, Jeffcoate WJ. A systematic review of the effectiveness of interventions to enhance the healing of chronic ulcers of the foot in diabetes. Diabetes Metab Res Rev. 2008 May-Jun;24 Suppl 1:S119-44.
Harry J. Anatomy and physiology of the skin. Br J Nurs. 2025 Aug 7;34(12):754-760.
Hong WX, Hu MS, Esquivel M, Liang GY, Rennert RC, McArdle A, Paik KJ, Duscher D, Gurtner GC, Lorenz HP, Longaker MT. The Role of Hypoxia-Inducible Factor in Wound Healing. Adv Wound Care (New Rochelle). 2014 May 1;3(5):390-399.
Huang C, Liu H, Yang Y, He Y, Shen W. Berberine suppressed the epithelial-mesenchymal transition (EMT) of colon epithelial cells through the TGF-β1/Smad and NF-κB pathways associated with miRNA-1269a. Heliyon. 2024 Aug 12;10(16):e36059.
Huang C, Wang XL, Qi FF, Pang ZL. Berberine inhibits epithelial-mesenchymal transition and promotes apoptosis of tumour-associated fibroblast-induced colonic epithelial cells through regulation of TGF-β signalling. J Cell Commun Signal. 2020 Mar;14(1):53-66.
Hui Y, Xu Z, Li J, Kuang L, Zhong Y, Tang Y, Wei J, Zhou H, Zheng T. Nonenzymatic function of DPP4 promotes diabetes-associated cognitive dysfunction through IGF-2R/PKA/SP1/ERp29/IP3R2 pathway-mediated impairment of Treg function and M1 microglia polarization. Metabolism. 2023 Jan;138:155340.
International Diabetes Federation. IDF Diabetes Atlas (11th ed). Brussels, Belgium: International Diabetes Federation; 2025.
Kalluri R, Weinberg RA. The basics of epithelial-mesenchymal transition. J Clin Invest. 2009 Jun;119(6):1420-8.
Kanitakis J. Anatomy, histology and immunohistochemistry of normal human skin. Eur J Dermatol. 2002 Jul-Aug;12(4):390-9; quiz 400-1.
Khalid M, Petroianu G, Adem A. Advanced Glycation End Products and Diabetes Mellitus: Mechanisms and Perspectives. Biomolecules. 2022 Apr 4;12(4):542.
Klemann C, Wagner L, Stephan M, von Hörsten S. Cut to the chase: a review of CD26/dipeptidyl peptidase-4's (DPP4) entanglement in the immune system. Clin Exp Immunol. 2016 Jul;185(1):1-21.
Knoedler S, Knoedler L, Kauke-Navarro M, Rinkevich Y, Hundeshagen G, Harhaus L, Kneser U, Pomahac B, Orgill DP, Panayi AC. Regulatory T cells in skin regeneration and wound healing. Mil Med Res. 2023 Oct 23;10(1):49.
Ko SY, Chang SS, Lin IH, Chen HI. Suppression of antioxidant Nrf-2 and downstream pathway in H9c2 cells by advanced glycation end products

(AGEs) via ERK phosphorylation. Biochimie. 2015 Nov;118:8-14.
Kolluru GK, Bir SC, Kevil CG. Endothelial dysfunction and diabetes: effects on angiogenesis, vascular remodeling, and wound healing. Int J Vasc Med. 2012;2012:918267.
Kruglikov IL, Scherer PE. Dermal Adipocytes: From Irrelevance to Metabolic Targets? Trends Endocrinol Metab. 2016 Jan;27(1):1-10.
Lambeir AM, Durinx C, Scharpé S, De Meester I. Dipeptidyl-peptidase IV from bench to bedside: an update on structural properties, functions, and clinical aspects of the enzyme DPP IV. Crit Rev Clin Lab Sci. 2003 Jun;40(3):209-94.
Lambeir AM, Proost P, Durinx C, Bal G, Senten K, Augustyns K, Scharpé S, Van Damme J, De Meester I. Kinetic investigation of chemokine truncation by CD26/dipeptidyl peptidase IV reveals a striking selectivity within the chemokine family. J Biol Chem. 2001 Aug 10;276(32):29839-45.
Lee JM, Veres SP. Advanced glycation end-product cross-linking inhibits biomechanical plasticity and characteristic failure morphology of native tendon. J Appl Physiol (1985). 2019 Apr 1;126(4):832-841.
Lendahl U, Muhl L, Betsholtz C. Identification, discrimination and heterogeneity of fibroblasts. Nat Commun. 2022 Jun 14;13(1):3409.
Li S, Fan Y, Kumagai A, Kawakita E, Kitada M, Kanasaki K, Koya D. Deficiency in Dipeptidyl Peptidase-4 Promotes Chemoresistance through the CXCL12/CXCR4/mTOR/TGFβ Signaling Pathway in Breast Cancer Cells. Int J Mol Sci. 2020 Jan 26;21(3):805.
Li Y, Huang H, Gu C, Huang W, Chen X, Lu X, You A, Ye S, Zhong J, Zhao Y, Yan Y, Li C. Film-forming polymer solutions containing cholesterol myristate and berberine mediate pressure ulcer repair via the Wnt/β-catenin pathway. Wound Repair Regen. 2024 May-Jun;32(3):279-291.
Liang CC, Park AY, Guan JL. In vitro scratch assay: a convenient and inexpensive method for analysis of cell migration in vitro. Nat Protoc. 2007;2(2):329-33.
Liu C, Rinderknecht H, Histing T, et al. Establishment of an In Vitro Scab Model for Investigating Different Phases of Wound Healing. Bioengineering (Basel). 2022;9(5):191.
Liu C, Rinderknecht H, Histing T, Kolbenschlag J, Nussler AK, Ehnert S. Establishment of an In Vitro Scab Model for Investigating Different Phases of Wound Healing. Bioengineering (Basel). 2022 Apr 28;9(5):191.
Liu CH, Tang WC, Sia P, Huang CC, Yang PM, Wu MH, Lai IL, Lee KH. Berberine inhibits the metastatic ability of prostate cancer cells by suppressing epithelial-to-mesenchymal transition (EMT)-associated genes with predictive and prognostic relevance. Int J Med Sci. 2015 Jan 1;12(1):63-71.
Liu D, Zhao H, Zhang Y, Hu J, Xu H. Efficacy and safety of berberine on the components of metabolic syndrome: a systematic review and meta-analysis of randomized placebo-controlled trials. Front Pharmacol. 2025 Jul

16;16:1572197.
Liu X, Liang Q, Wang Y, Xiong S, Yue R. Advances in the pharmacological mechanisms of berberine in the treatment of fibrosis. Front Pharmacol. 2024 Sep 20;15:1455058.
Liu Y, Petreaca M, Martins-Green M. Cell and molecular mechanisms of insulin-induced angiogenesis. J Cell Mol Med. 2009 Nov-Dec;13(11-12):4492-504.
Liu YT, Hao HP, Xie HG, Lai L, Wang Q, Liu CX, Wang GJ. Extensive intestinal first-pass elimination and predominant hepatic distribution of berberine explain its low plasma levels in rats. Drug Metab Dispos. 2010 Oct;38(10):1779-84.
Lobmann R, Zemlin C, Motzkau M, Reschke K, Lehnert H. Expression of matrix metalloproteinases and growth factors in diabetic foot wounds treated with a protease absorbent dressing. J Diabetes Complications. 2006 Sep-Oct;20(5):329-35.
Long M, Cai L, Li W, Zhang L, Guo S, Zhang R, Zheng Y, Liu X, Wang M, Zhou X, Wang H, Li X, Li L, Zhu Z, Yang G, Zheng H. DPP-4 Inhibitors Improve Diabetic Wound Healing via Direct and Indirect Promotion of Epithelial-Mesenchymal Transition and Reduction of Scarring. Diabetes. 2018 Mar;67(3):518-531.
Lustig S, Maik-Rachline G, Paran N, Melamed S, Israely T, Erez N, Orr N, Reuveny S, Ordentlich A, Laub O, Shafferman A, Velan B. Effective post-exposure protection against lethal orthopoxviruses infection by vaccinia immune globulin involves induction of adaptive immune response. Vaccine. 2009 Mar 10;27(11):1691-9.
Lv H, Wang S, He M, Zhu X, He P, Sun R, Jia Z, Wang Z, Zhao W, Zhong Z, Han Y. Electrospun SF/PHBV nanofibers loaded with berberine as a bioactive wound dressing: Accelerating diabetic wound healing and alleviating hypertrophic scar. Materials & Design. 2024;251:113574.
Maksimovic S, Nakatani M, Baba Y, Nelson AM, Marshall KL, Wellnitz SA, Firozi P, Woo SH, Ranade S, Patapoutian A, Lumpkin EA. Epidermal Merkel cells are mechanosensory cells that tune mammalian touch receptors. Nature. 2014 May 29;509(7502):617-21.
Marfella R, Sasso FC, Rizzo MR, Paolisso P, Barbieri M, Padovano V, Carbonara O, Gualdiero P, Petronella P, Ferraraccio F, Petrella A, Canonico R, Campitiello F, Della Corte A, Paolisso G, Canonico S. Dipeptidyl peptidase 4 inhibition may facilitate healing of chronic foot ulcers in patients with type 2 diabetes. Exp Diabetes Res. 2012;2012:892706.
Marguet D, Baggio L, Kobayashi T, Bernard AM, Pierres M, Nielsen PF, Ribel U, Watanabe T, Drucker DJ, Wagtmann N. Enhanced insulin secretion and improved glucose tolerance in mice lacking CD26. Proc Natl Acad Sci U S A. 2000 Jun 6;97(12):6874-9.
Merkt W, Zhou Y, Han H, Lagares D. Myofibroblast fate plasticity in tissue repair and fibrosis: Deactivation, apoptosis, senescence and

reprogramming. Wound Repair Regen. 2021 Jul;29(4):678-691.
Michopoulou A, Montmasson M, Garnier C, Lambert E, Dayan G, Rousselle P. A novel mechanism in wound healing: Laminin 332 drives MMP9/14 activity by recruiting syndecan-1 and CD44. Matrix Biol. 2020 Dec;94:1-17.
Mirza RE, Koh TJ. Contributions of cell subsets to cytokine production during normal and impaired wound healing. Cytokine. 2014.
Mizukoshi K, Kurosumi M, Hamanaka Y. Age-related changes in the fiber structure around adipocytes in the subcutaneous fat layer and their association with skin viscoelasticity. Skin Res Technol. 2024 Feb;30(2):e13566.
Mori N, Oda K, Takakura H, Tanaka Y, Yokooji T, Murakami T. Comparison of Berberine Bioavailability between Oral and Rectal Administrations in Rats. Biol Pharm Bull. 2023;46(11):1639-1642.
Moustakas A, Heldin CH. Induction of epithelial-mesenchymal transition by transforming growth factor β. Semin Cancer Biol. 2012 Oct;22(5-6):446-54.
Muller M, Trocme C, Lardy B, Morel F, Halimi S, Benhamou PY. Matrix metalloproteinases and diabetic foot ulcers: the ratio of MMP-1 to TIMP-1 is a predictor of wound healing. Diabet Med. 2008 Apr;25(4):419-26.
Mulvihill EE, Drucker DJ. Pharmacology, physiology, and mechanisms of action of dipeptidyl peptidase-4 inhibitors. Endocr Rev. 2014 Dec;35(6):992-1019.
Nathan C. Neutrophils and immunity: challenges and opportunities. Nat Rev Immunol. 2006 Mar;6(3):173-82.
Neag MA, Mocan A, Echeverría J, Pop RM, Bocsan CI, Crişan G, Buzoianu AD. Berberine: Botanical Occurrence, Traditional Uses, Extraction Methods, and Relevance in Cardiovascular, Metabolic, Hepatic, and Renal Disorders. Front Pharmacol. 2018 Aug 21;9:557.
Nestle FO, Di Meglio P, Qin JZ, Nickoloff BJ. Skin immune sentinels in health and disease. Nat Rev Immunol. 2009 Oct;9(10):679-91.
Nieto MA, Huang RY, Jackson RA, Thiery JP. EMT: 2016. Cell. 2016;166(1):21-45.
Novak ML, Koh TJ. Phenotypic transitions of macrophages orchestrate tissue repair. Am J Pathol. 2013 Nov;183(5):1352-1363.
Nowak NC, Menichella DM, Miller R, Paller AS. Cutaneous innervation in impaired diabetic wound healing. Transl Res. 2021 Oct;236:87-108.
Ogawa R, Akaishi S, Huang C, Dohi T, Aoki M, Omori Y, Koike S, Kobe K, Akimoto M, Hyakusoku H. Clinical applications of basic research that shows reducing skin tension could prevent and treat abnormal scarring: the importance of fascial/subcutaneous tensile reduction sutures and flap surgery for keloid and hypertrophic scar reconstruction. J Nippon Med Sch. 2011;78(2):68-76.
Okonkwo UA, DiPietro LA. Diabetes and Wound Angiogenesis. Int J Mol Sci. 2017 Jul 3;18(7):1419.
Pan GY, Wang GJ, Liu XD, Fawcett JP, Xie YY. The involvement of

P-glycoprotein in berberine absorption. Pharmacol Toxicol. 2002 Oct;91(4):193-7.
Panda DS, Eid HM, Elkomy MH, Khames A, Hassan RM, Abo El-Ela FI, Yassin HA. Berberine Encapsulated Lecithin-Chitosan Nanoparticles as Innovative Wound Healing Agent in Type II Diabetes. Pharmaceutics. 2021 Aug 4;13(8):1197.
Papakonstantinou E, Roth M, Karakiulakis G. Hyaluronic acid: A key molecule in skin aging. Dermatoendocrinol. 2012 Jul 1;4(3):253-8.
Pastar I, Stojadinovic O, Yin NC, Ramirez H, Nusbaum AG, Sawaya A, Patel SB, Khalid L, Isseroff RR, Tomic-Canic M. Epithelialization in Wound Healing: A Comprehensive Review. Adv Wound Care (New Rochelle). 2014 Jul 1;3(7):445-464.
Peña OA, Martin P. Cellular and molecular mechanisms of skin wound healing. Nat Rev Mol Cell Biol. 2024 Aug;25(8):599-616.
Peinado H, Olmeda D, Cano A. Snail, Zeb and bHLH factors in tumour progression: an alliance against the epithelial phenotype? Nat Rev Cancer. 2007 Jun;7(6):415-28.
Pfeiffenberger, M., et al. (2019). "Hypoxia and mesenchymal stromal cells as key drivers of initial fracture healing in an equine in vitro fracture hematoma model." Plos One 14(4): e0214276.
Rinderknecht H, Mayer A, Histing T, Ehnert S, Nüssler A. Herbal Extracts of Ginseng and Maqui Berry Show Only Minimal Effects on an In Vitro Model of Early Fracture Repair of Smokers. Foods. 2023 Aug 4;12(15):2960.
Rinderknecht H, Nussler AK, Steinestel K, Histing T, Ehnert S. Smoking Impairs Hematoma Formation and Dysregulates Angiogenesis as the First Steps of Fracture Healing. Bioengineering (Basel). 2022 Apr 24;9(5):186.
Rittié L, Sachs DL, Orringer JS, Voorhees JJ, Fisher GJ. Eccrine sweat glands are major contributors to reepithelialization of human wounds. Am J Pathol. 2013 Jan;182(1):163-71.
Romani N, Clausen BE, Stoitzner P. Langerhans cells and more: langerin-expressing dendritic cell subsets in the skin. Immunol Rev. 2010 Mar;234(1):120-41.
Rosen ED, Spiegelman BM. Adipocytes as regulators of energy balance and glucose homeostasis. Nature. 2006 Dec 14;444(7121):847-53.
Saeedi P, Salpea P, Karuranga S, Petersohn I, Malanda B, Gregg EW, Unwin N, Wild SH, Williams R. Mortality attributable to diabetes in 20-79 years old adults, 2019 estimates: Results from the International Diabetes Federation Diabetes Atlas, 9th edition. Diabetes Res Clin Pract. 2020 Apr;162:108086.
Sahin F, Breinbauer R, Linnemann C, Tombaz M, Nussler AK, Ehnert S. Quantification of Circulating Cell-Free DNA as a NETosis Marker in Trauma Patients with Type 2 Diabetes Mellitus. Methods Protoc. 2025 Apr 16;8(2):42.
Sandby-Møller J, Poulsen T, Wulf HC. Epidermal thickness at different body sites: relationship to age, gender, pigmentation, blood content, skin type

and smoking habits. Acta Derm Venereol. 2003;83(6):410-3.
Schultz GS, Wysocki A. Interactions between extracellular matrix and growth factors in wound healing. Wound Repair Regen. 2009 Mar-Apr;17(2):153-62.
Schäfer M, Werner S. Oxidative stress in normal and impaired wound repair. Pharmacol Res. 2008 Aug;58(2):165-71.
Schürmann C, Linke A, Engelmann-Pilger K, Steinmetz C, Mark M, Pfeilschifter J, Klein T, Frank S. The dipeptidyl peptidase-4 inhibitor linagliptin attenuates inflammation and accelerates epithelialization in wounds of diabetic ob/ob mice. J Pharmacol Exp Ther. 2012 Jul;342(1):71-80.
Segre JA. Epidermal barrier formation and recovery in skin disorders. J Clin Invest. 2006 May;116(5):1150-8.
Shahin H, Steinvall I, Sjöberg F, Elmasry M, El-Serafi A. Towards propagation of epidermal cells for wound repair: glass, as cell culture substrate, enhances proliferation and migration of human keratinocytes. Front Bioeng Biotechnol. 2025 Mar 20;13:1547044.
Sharun K, Banu SA, Mamachan M, Subash A, Karikalan M, Kumar R, Vinodhkumar OR, Dhama K, Pawde AM, Amarpal. Development and characterization of contraction-suppressed full-thickness skin wound model in rabbits. Tissue Cell. 2024 Oct;90:102482.
Shteingauz A, Porat Y, Voloshin T, Schneiderman RS, Munster M, Zeevi E, Kaynan N, Gotlib K, Giladi M, Kirson ED, Weinberg U, Kinzel A, Palti Y. AMPK-dependent autophagy upregulation serves as a survival mechanism in response to Tumor Treating Fields (TTFields). Cell Death Dis. 2018 Oct 19;9(11):1074.
Sinagra T, Merlo S, Spampinato SF, Pasquale RD, Sortino MA. High mobility group box 1 contributes to wound healing induced by inhibition of dipeptidylpeptidase 4 in cultured keratinocytes. Front Pharmacol. 2015 Jun 16;6:126.
Singh K, Sinha M, Pal D, Tabasum S, Gnyawali SC, Khona D, Sarkar S, Mohanty SK, Soto-Gonzalez F, Khanna S, Roy S, Sen CK. Cutaneous Epithelial to Mesenchymal Transition Activator ZEB1 Regulates Wound Angiogenesis and Closure in a Glycemic Status-Dependent Manner. Diabetes. 2019 Nov;68(11):2175-2190.
Singh N, Armstrong DG, Lipsky BA. Preventing foot ulcers in patients with diabetes. JAMA. 2005;293(2):217-228.
Sotomayor S, Pascual G, Blanc-Guillemaud V, Mesa-Ciller C, García-Honduvilla N, Cifuentes A, Buján J. Effects of a novel NADPH oxidase inhibitor (S42909) on wound healing in an experimental ischemic excisional skin model. Exp Dermatol. 2017 Feb;26(2):148-155.
Stemmler MP, Eccles RL, Brabletz S, Brabletz T. Non-redundant functions of EMT transcription factors. Nat Cell Biol. 2019;21(1):102-112.
Sullivan TP, Eaglstein WH, Davis SC, Mertz P. The pig as a model for human

wound healing. Wound Repair Regen. 2001 Mar-Apr;9(2):66-76.
Summerfield A, Meurens F, Ricklin ME. The immunology of the porcine skin and its value as a model for human skin. Mol Immunol. 2015 Jul;66(1):14-21.
Sun K, Li X, Scherer PE. Extracellular Matrix (ECM) and Fibrosis in Adipose Tissue: Overview and Perspectives. Compr Physiol. 2023 Jan 30;13(1):4387-4407.
Sun X, Joost S, Kasper M. Plasticity of Epithelial Cells during Skin Wound Healing. Cold Spring Harb Perspect Biol. 2023 May 2;15(5):a041232.
Uitto J, Bernstein EF. Molecular mechanisms of cutaneous aging: connective tissue alterations in the dermis. J Investig Dermatol Symp Proc. 1998 Aug;3(1):41-4.
Uitto J, Olsen DR, Fazio MJ. Extracellular matrix of the skin: 50 years of progress. J Invest Dermatol. 1989 Apr;92(4 Suppl):61S-77S.
Verhaegen PD, van Zuijlen PP, Pennings NM, van Marle J, Niessen FB, van der Horst CM, Middelkoop E. Differences in collagen architecture between keloid, hypertrophic scar, normotrophic scar, and normal skin: An objective histopathological analysis. Wound Repair Regen. 2009 Sep-Oct;17(5):649-56.
Vinik AI, Erbas T, Park TS, Stansberry KB, Scanelli JA, Pittenger GL. Dermal neurovascular dysfunction in type 2 diabetes. Diabetes Care. 2001 Aug;24(8):1468-75.
Wang H, Zhu C, Ying Y, Luo L, Huang D, Luo Z. Metformin and berberine, two versatile drugs in treatment of common metabolic diseases. Oncotarget. 2017 Sep 11;9(11):10135-10146.
Weinstein GD, McCullough JL, Ross P. Cell proliferation in normal epidermis. J Invest Dermatol. 1984 Jun;82(6):623-8.
Wells JC. Sexual dimorphism of body composition. Best Pract Res Clin Endocrinol Metab. 2007 Sep;21(3):415-30.
Werner S, Grose R. Regulation of wound healing by growth factors and cytokines. Physiol Rev. 2003 Jul;83(3):835-70.
Wheater PR, Burkitt HG, Daniels VG. Functional histology: a text and colour atlas. 2nd ed. Edinburgh: Churchill Livingstone; 1987.
Whittam AJ, Maan ZN, Duscher D, Barrera JA, Hu MS, Fischer LH, Khong S, Kwon SH, Wong VW, Walmsley GG, Giacco F, Januszyk M, Brownlee M, Longaker MT, Gurtner GC. Small molecule inhibition of dipeptidyl peptidase-4 enhances bone marrow progenitor cell function and angiogenesis in diabetic wounds. Transl Res. 2019 Mar;205:51-63.
Wolberg AS. Fibrinogen and fibrin: synthesis, structure, and function in health and disease. J Thromb Haemost. 2023 Nov;21(11):3005-3015.
Xue M, Jackson CJ. Extracellular Matrix Reorganization During Wound Healing and Its Impact on Abnormal Scarring. Adv Wound Care (New Rochelle). 2015 Mar 1;4(3):119-136.
Yamaguchi Y, Hearing VJ. Melanocytes and their diseases. Cold Spring Harb

Perspect Med. 2014 May 1;4(5):a017046.
Yin J, Qin S, Chen J, Wong N, Peng C, Li D. Berberine-based strategies: novel delivery systems bring out new potential for wound healing. Chin Med. 2025 Oct 1;20(1):150.
Zhang J, Zhou R, Xiang C, Jia Q, Wu H, Yang H. Huangbai Liniment Accelerated Wound Healing by Activating Nrf2 Signaling in Diabetes. Oxid Med Cell Longev. 2020 May 23;2020:4951820.
Zhang JJ, Zhou R, Deng LJ, Cao GZ, Zhang Y, Xu H, Hou JY, Ju S, Yang HJ. Huangbai liniment and berberine promoted wound healing in high-fat diet/Streptozotocin-induced diabetic rats. Biomed Pharmacother. 2022 Jun;150:112948.
Zhang KW, Liu SY, Jia Y, Zou ML, Teng YY, Chen ZH, Li Y, Guo D, Wu JJ, Yuan ZD, Yuan FL. Insight into the role of DPP-4 in fibrotic wound healing. Biomed Pharmacother. 2022 Jul;151:113143.
Zhang P, Sun Y, Ma L. ZEB1: at the crossroads of epithelial-mesenchymal transition, metastasis and therapy resistance. Cell Cycle. 2015;14(4):481-7.
Zhang Y, Do KK, Wang F, Lu X, Liu JY, Li C, Ceresa BP, Zhang L, Dean DC, Liu Y. Zeb1 facilitates corneal epithelial wound healing by maintaining corneal epithelial cell viability and mobility. Commun Biol. 2023 Apr 20;6(1):434.
Zhang Y, Li X, Zou D, Liu W, Yang J, Zhu N, Huo L, Wang M, Hong J, Wu P, Ren G, Ning G. Treatment of type 2 diabetes and dyslipidemia with the natural plant alkaloid berberine. J Clin Endocrinol Metab. 2008 Jul;93(7):2559-65.
Zhou R, Xiang C, Cao G, Xu H, Zhang Y, Yang H, Zhang J. Berberine accelerated wound healing by restoring TrxR1/JNK in diabetes. Clin Sci (Lond). 2021 Feb 12;135(4):613-627.

8. Appendix A

Molecular effects of BBR on gene expression in control scabs

We further evaluated the effects of BBR on Ctrl scabs to assess its impact on normal wound healing physiology (Figures A1–A3). Representative gel images analysis demonstrated dose-dependent effects of BBR on gene expression in control scabs (Figure A1A). Semiquantitative PCR analysis showed that *DPP4* mRNA levels were reduced in BBR-treated groups compared with the 0 μM control, in a dose-dependent manner (Figure A1B). Analysis of epithelial markers revealed that *E-cadherin* expression was significantly downregulated at 50 μM ($p < 0.05$) (Figure A1C). *Keratin 18* expression was significantly upregulated at 100 μM ($p < 0.001$) (Figure A1D), while *Keratin 19* showed a dose-dependent increasing trend (Figure A1E).

Representative gel images analysis demonstrated dose-dependent effects of BBR on mesenchymal marker expression (Figure A2A). Assessment of mesenchymal markers demonstrated that *N-cadherin* expression was significantly upregulated at both 50 μM ($p < 0.05$) and 100 μM ($p < 0.0001$) (Figure A2B). *Vimentin* exhibited an increasing trend following BBR treatment (Figure A2C), whereas *Fibronectin* showed no statistically significant changes across the tested concentrations (Figure A2D).

Representative gel images analysis demonstrated dose-dependent effects of BBR on EMT transcription factor expression (Figure A3A). Finally, analysis of EMT transcription factors revealed complex regulatory patterns. *Snail1* expression was reduced at 50 μM but elevated at 100 μM compared with the 0 μM group (Figure A3B). *Snail2* levels were significantly higher at 100 μM ($p < 0.05$) (Figure A3C). *ZEB1* showed a significant dose-dependent increase (50 μM: $p < 0.01$; 100 μM: $p < 0.0001$) (Figure A3D). Notably, *ZEB2* expression was significantly suppressed at 50 μM ($p < 0.01$) but partially recovered at 100 μM (Figure A3E).

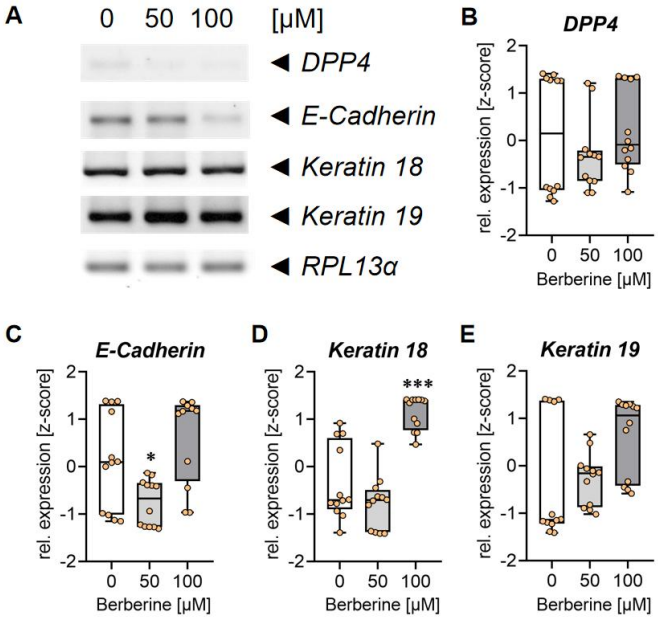


Figure A1: Effects of BBR on *DPP4* and epithelial marker expression in control scabs. Semiquantitative PCR analysis of gene expression in control scabs treated with BBR (0, 50, or 100 µM) on Day 2. (A) Representative gel images showing expression of *DPP4*, *E-cadherin*, *Keratin 18*, *Keratin 19*, and *RPL13α* (loading control) at different BBR concentrations. Relative expression (z-score) is shown for (B) *DPP4*, (C) *E-cadherin*, (D) *Keratin 18*, and (E) *Keratin 19*. Statistical significance was determined by Kruskal-Wallis test. *p < 0.05, ***p < 0.001 vs 0 µM BBR.

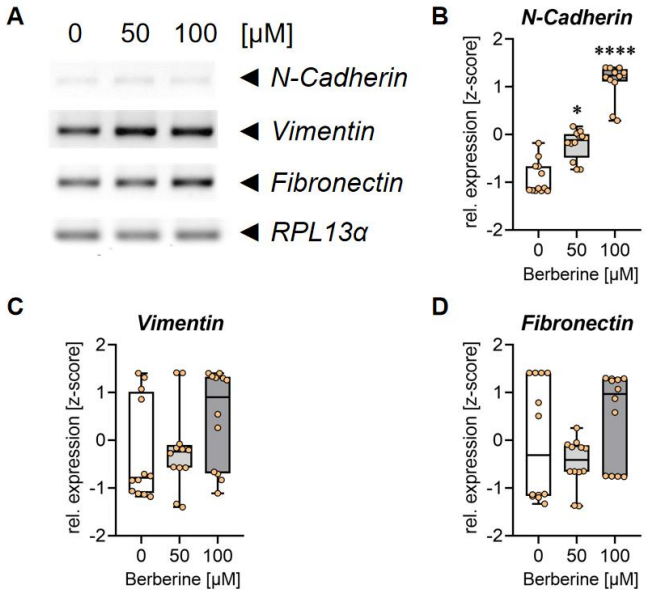


Figure A2: Effects of BBR on mesenchymal marker expression in control scabs. Semiquantitative PCR analysis of mesenchymal markers in control scabs treated with BBR (0, 50, or 100 µM) on Day 2. (A) Representative gel images showing expression of *N-cadherin*, *Vimentin*, *Fibronectin*, and *RPL13α* (loading control) at different BBR concentrations. Relative expression (z-score) is shown for (B) *N-cadherin*, (C) *Vimentin*, and (D) *Fibronectin*. Statistical

significance was determined by Kruskal-Wallis test. *p < 0.05, ****p < 0.0001 vs 0 µM BBR.

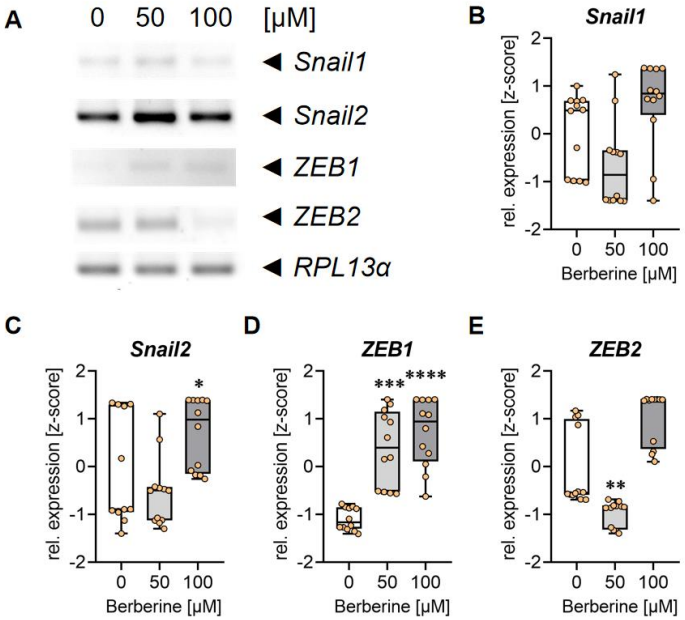


Figure A3: Effects of BBR on EMT transcription factor expression in control scabs. Semiquantitative PCR analysis of EMT-regulating transcription factors in control scabs treated with BBR (0, 50, or 100 µM) on Day 2. (A) Representative gel images showing expression of *Snail1*, *Snail2*, *ZEB1*, *ZEB2*, and *RPL13α* (loading control) at different BBR concentrations. Relative expression (z-score) is shown for (B) *Snail1*, (C) *Snail2*, (D) *ZEB1*, and (E) *ZEB2*. Statistical significance was determined by Kruskal-Wallis test. *p < 0.05, **p < 0.01, ****p < 0.0001 vs 0 µM BBR.

9. Declaration

This study was performed entirely at Siegfried Weller Institute under the guidance of Prof. Dr. Andreas Nüssler and Prof. Dr. Sabrina Ehnert.

Prof. Dr. Sabrina Ehnert and I designed the experiments. All experiments were conducted by myself, and all analyses were completed under the guidance of the Prof. Dr. Sabrina Ehnert.

All presented data are derived from our original work, except for the quoted references and figures.

I hereby declare that the submitted thesis entitled: “Effects of Berberine, a Natural Plant-Derived DPP4 Inhibitor, on *In Vitro* Scab Remodeling” has not been submitted in any application for a degree.

10. Publication

The publication of the presented data is planned. The preparation of the manuscript is currently ongoing.

11. Acknowledgement

To my mother: I wish you were here, I know you would be proud of me. To my father, who opened up a wider world for me.

I would like to express my sincere gratitude to my supervisor Prof. Dr. Sabrina Ehnert, for her continuous support and guidance throughout this research journey. I am also deeply grateful to Prof. Dr. Andreas Nüssler for his encouragement and advice. I am deeply grateful for your dedicated mentorship, invaluable advice, and assistance over the past three years of my doctoral studies.

I would also like to extend my special thanks to someone very dear to me. Thank you, Linger T, for your unwavering and gentle support throughout my doctoral journey and during the writing of this dissertation. Your presence made this journey, which could have been lonely, filled with warmth and quiet strength. I am truly grateful to have you walking beside me at such an important chapter of my life.

I would like to thank all members of the Siegfried Weller Institut (SWI). I have been fortunate to meet many remarkable people along the way.

My final thanks goes to myself. Until we meet again, adventurer.

The breeze of freedom travels with me as I continue forward, walking toward the glow of a thousand lights.

Blessed that our paths crossed. May our journey ahead be long yet luminous.